Methods for Modeling the Dynamic Mass Flows in a Large Two-Stroke Diesel Engine with EGR

Master Thesis

$$(EIv'')'' = q - \rho A \ddot{v}$$

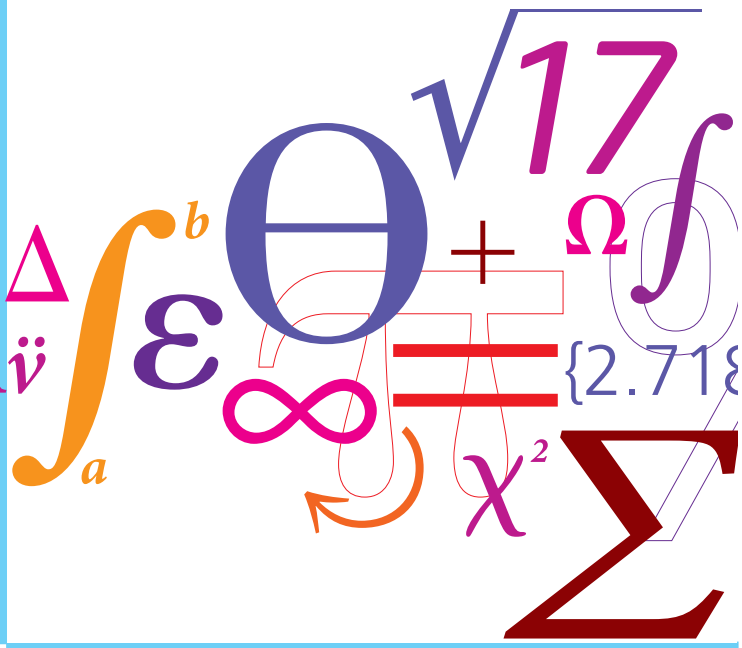

Guillem Alegret Nadal
April 2014

DTU Mechanical Engineering
Department of Mechanical Engineering

GUILLEM ALEGRET NADAL (S111176)

Methods for Modeling the Dynamic Mass Flows in a Large Two-Stroke Diesel Engine with EGR

Master's Thesis, April 2014

Supervisors:

Jesper Schramm, Lector at the Mechanical Engineering Department of DTU

Mogens Blanke, Professor at the Electrical Engineering Department of DTU

Morten Vejlgaard-Laursen, Head of the Control Technology Department, MAN Diesel&Turbo

DTU - Technical University of Denmark, Kgs. Lyngby - 2014

Methods for Modeling the Dynamic Mass Flows in a Large Two-Stroke Diesel Engine with EGR

This report was prepared by:
Guillem Alegret Nadal (s111176)

Advisors:
Jesper Schramm, Lector at the Mechanical Engineering Department of DTU
Mogens Blanke, Professor at the Electrical Engineering Department of DTU
Morten Vejlgaard-Laursen, Head of the Control Technology Department, MAN Diesel&Turbo

DTU Mechanical Engineering
Technical University of Denmark
Nils Koppels Allé
Building 404
2800 Kgs. Lyngby
Denmark
Tel: +45 4525 1960

Project period: December 2013- April 2014

ECTS: 30

Education: MSc

Field: Mechanical and Electrical Engineering

Class: Public

Remarks: This report is submitted as partial fulfillment of the requirements for graduation in the above education at the Technical University of Denmark.

Table of Contents

List of Figures

List of Tables

Abstract

In this project different methods to model two-stroke diesel engines have been investigated. The goal of the project is to obtain a model capable to capture both the steady states and the transients of the engine system. The interest MAN Diesel&Turbo has in this model is to obtain a reliable simulation platform to be used as a tool to evaluate the performance of new control systems for the Exhaust Gas Recirculation (EGR) system.

A non-linear model of the engine air-path with EGR is derived and validated against measurements. The specific engine corresponds to a 4T50ME-X located at MAN Diesel&Turbo research center. The model consists of the following components: the turbocharger, the scavenging and exhaust manifolds, the cylinders and the EGR system.

The turbocharger model is externalized to an advance simulator software (GT-Power), all other components are modeled in Simulink. A Seiliger cycle capable of handling variable exhaust valve opening and closing is proposed. The polytropic coefficients for the compression and expansion are analytically estimated from in-cylinder pressure measurements.

The model derived in this project is capable to fit well the measured data in steady states. The appropriate dynamics are obtained in transient operations, although the model shows a generalized faster response than the measured data.

Acknowledgments

This project has been performed at the Technical University of Denmark (DTU), in close collaboration with MAN Diesel & Turbo.

I would like to thank my supervisors Jesper Scamm and Mogens Blanke for the support and guidance. I would also like to thank my supervisor at MAN Diesel&Turbo Morten Vejlgaard-Laursen for his endless help in understanding the system. My colleagues at MAN Diesel & Turbo: Nicolai Pedersen, Claes Zander and Casper Svendsen for the long discussions and clarifications of the system; and Zeljko Stojakovic for all his help with GT-Power; Lars Erikson for the possibility to use the software CHEPP; and Salvador Pineda for helping out with the English language.

And finally I would like to thank my family and my girlfriend Ariadna Marin for the moral support during all the thesis.

Copenhaguen, April 2014
Guillem Alegret Nadal

CHAPTER 1

Introduction

The model presented in this project corresponds to a large two-stroke marine diesel engine. This kind of engines are mainly found in marine vessels. More than 90% of global trade is done by sea, and the tendency shows that the amount of goods being transported by sea is in continuous rise (UNCTAD 2013).

The International Marine Organization (IMO) is an agency of the United Nations in charge of preventing marine pollution. Tier I and II are regulations issued by this agency in the past years, 2000 and 2011 respectively IMO (2011). These regulations establish emission limits for maritime diesel engines concerning NO_x and SO_x. In 2016 the Tier III regulation will be issued. The upcoming Tier III will only apply to vessels sailing inside the Emission Control Areas IMO (2011) and it will only apply to NO_x emissions. It will establish the NO_x emission reduction by 80% from current limit values.

To fulfill the requirements of Tier III, dedicated NO_x emission control technologies are required. The main technologies that are currently used for NO_x reduction are the following: water injection into the combustion process, Selective Catalytic Reduction and Exhaust Gas Recirculation (EGR).

This project will be focused on the EGR technology. As its name indicates, this technology is based on recirculating the combustion products to reduce the oxygen content of the charge. Since NO_x formation is directly correlated to the peak temperature reached in the combustion (Lamas and Rodríguez 2012), inducing a lower oxygen content in the charge results in a slower combustion and consequently in a lower combustion peak temperature.

1.1 Purpose

The Tier III regulation is the next milestone for EGR technology. To fulfill the new limitations higher recirculated flows are demanded compared to Tier II and thus, more advance controllers are needed. Due to the high economical costs of performing tests on the real engine, a reliable dynamic engine model is an important tool in the development of new EGR control systems. Therefore the purpose of this project is to develop a model of the air-path system capable of capturing the steady states as well as dynamics of the system during transients operations.

1.2 Literature review

Different approaches for modeling the engine air-path system found in literature are mainly targeting 4-stroke engines (Heywood 1988), (Guzzella and Onder 2010) and (Sorenson 2008). Specific research within exhaust gas recirculation is also mainly based on 4-stroke automotive engines Wahlström and Eriksson (2011) and (Vigild 2001). The most common modeling approach found in literature is the Mean Value Engine Model (MVEM).

Not much research has been dedicated towards large two stroke diesel engines, in which the exhaust valve opening and closing is regulated and the scavenging process differs significantly.

More literature regarding specific components of the system: an approach to parameterize performance maps is provided is (Eriksson 2007), research on the scavenging process of large two stroke engines is presented in (Andersen et al. 2013), a model of the Seiliger cycle from a thermodynamic point of view is derived in Byungchan Lee and van Nieuwstadt (2013).

Literature based on modeling engines with the same size as a 4T50ME-X is listed below:

- (Theotokatos 2010) presented a model of a marine two stroke diesel engine with two different modeling approaches.
- (Noppenau 2012) modeled a large diesel engine with SCR technology.
- (Tao 2012) presented a model of the air-path system with EGR for the 4T50ME-X engine, although it was proven to be valid only in certain operational ranges.
- (Mahler 2013) derived a MVEM of the 4T50ME-X engine with EGR technology. The derived model matched the measured data at 40% and 100% load, whereas a bias was obtained at 75% load.
- (Pedersen 2013) implemented a non-linear black box model of the entire system, although it proved to be really dependent on the identification dataset used. In this project the model presented by (Mahler 2013) was further improved, i.e. the turbine efficiency was considered in the model. But the same bias was obtained at 75% load.

1.3 Project scope

This project starts from the models presented by (Mahler 2013) and (Pedersen 2013). As recommended in (Pedersen 2013), special emphasis is taken towards improving the turbocharger submodel and also to include the EGR blower diffuser in the model.

The differences between 4-stroke and 2-stroke engines are studied in order to adapt modeling approaches based on 4-stroke engines.

The modeling complexity of each component in the system is intended to be consistent with the other components as well as with the overall complexity of a MVEM.

1.4 Structure of the document

- Chapter 2 gives a detailed description of the system considered in this document.
- Chapter 3 describes the modeling approach used in each of considered air-path components.
- Chapter 4 contains the determination of the model parameters.
- Chapter 5 gives an overview of the chronological evolution of the model, the parameters which need to be estimated from measured data are also tuned in this chapter.
- Chapter 6 presents the simulation results obtained with the model derived in chapter 3, measurements are used to validate the model.
- Chapter 7 explains the conclusions of the project and further work.

CHAPTER 2

System description

The specific engine modeled in this project corresponds to the test engine located at MAN Diesel&Turbo research center in Copenhagen. The engine is smaller than most of the engines found in the 2-stroke and slow speed MAN catalog and corresponds to the 4T50ME-X. The engine specifications which are relevant for the model are shown in Table 2.1. The power and speed at Maximum Continuous Rating (MCR) are shown as a reference for comparative purposes with other marine engines.

Number of cylinders	4	[-]
Stroke	2.2	[m]
Bore	0.5	[m]
Connecting Rod length	2.98	[m]
MCR Power	7800	[kW]
MCR Engine Speed	123	[RPM]

Table 2.1: Engine specifications

The engine corresponds to a turbocharged 2-stroke diesel engine with direct injection. A relevant advantage of a turbocharged engine is the negative pressure difference in the engine, the inlet has a higher pressure than the outlet, thus allowing a more effective scavenging process. In this engine the scavenging process is carried with uniflow scavenging method, which has a high scavenging efficiency. To have an overview of the complete system, Figure 2.1 shows the layout of all the components involved.

The Engine Control System (ECS) is the main controller in the engine. Some of its functions are: to maintain the desired scavenging pressure, to perform the injection of fuel and also to regulate the compression ratio. The ECS has an internal state called Engine Running Mode (ERM) which indicates how the engine is running. Moreover, there are 4 different running modes, although only two are present in the experimental data used in this project, ERM = 2 which indicates that the EGR system in not active, and ERM = 3 that indicates the EGR system is active. The engine running mode will be of special interest in section 3.2.4.

In section 2.1 the functionality of all the components is described, excluding the components of the EGR system which will be introduced in section 2.2. The components are presented with the same order as the flow stream. Some of components will not be considered in the model, but a good understanding of their functionality is needed to ensure consistency in the simplifications taken.

2.1 Air Path components

The atmospheric air enters the system through the preheater which ensures a constant temperature of the air at the compressor inlet. The purpose of preheating the atmospheric air is to be able to perform comparable

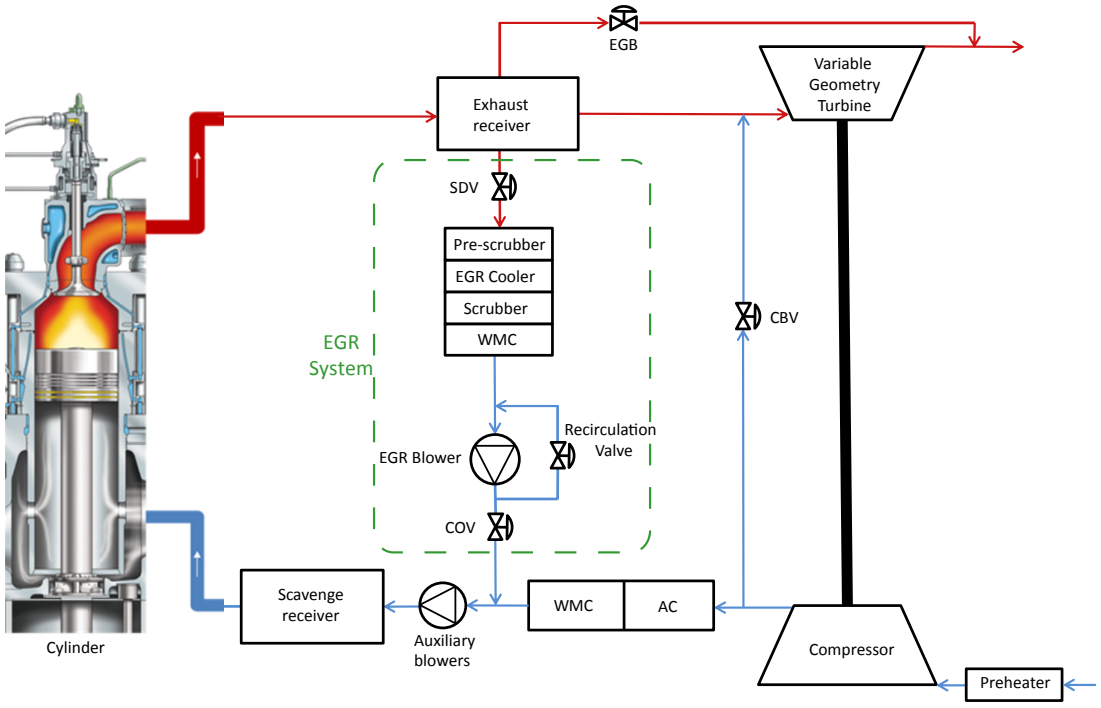

Figure 2.1: Components of the engine air path system found in 4T50ME-X

tests regardless of ambient conditions. The preheater is not considered in the model but the temperature in the compressor inlet is assumed to be constant.

Next the compressor raises the pressure and temperature of the air. The temperature is then decreased in the Air Cooler (AC) before entering into the scavenging manifold. The Air Cooling (AC) unit is responsible for maintaining a constant scavenging manifold temperature independently of the mass flow. A Water Mist Catcher (WMC) is installed after the AC to remove any water droplets condensed in the cooling process.

The auxiliary blowers are only needed in situations when the scavenging pressure is too low to perform the scavenging process properly. The Engine Control System (ECS) activates the auxiliary blowers when the scavenging pressure reaches a minimum threshold. The threshold is normally reached at load ranges lower than 30%. The auxiliary blowers will not be part of the model.

The air remains in the scavenging receiver before entering into one of the cylinders. The scavenging manifold is defined as the sum of the volumes of the components between the compressor and the cylinders. The volumes included are the AC, the WMC, the receiver, the scavenge air box and all the piping in between those components.

When the scavenging ports are unblocked, the gas enters into the cylinder replacing the combustion products of the previous stroke. Then the combustion chamber is sealed and the combustion occurs. The cylinder block will include the four cylinders with the respective pistons, exhaust valves and injection nozzles. The main difference with a common 2-stroke engine is that the exhaust valves are electronically controlled by the ECS, using high pressure hydraulics. The engine efficiency can be increased with the adequate control of the opening and closing of the exhaust valve.

When the exhaust valve opens the products are released into the exhaust receiver. The exhaust manifold includes the volume of the exhaust receiver and the piping. The volume of the EGR components is not included in any of the manifolds since in many situations it is not used.

The turbine is driven by the hot exhaust gases present in the receiver, recovering the residual energy

present in the exhaust gases. A nozzle ring equipped with adjustable vanes is mounted in the turbine inlet, therefore the turbocharger is referred as a Variable Geometry Turbocharger (VGT). The purpose of adjusting the pitch of the vanes is to vary the exhaust gas pressure and the amount of mass flow, which consequently modifies the amount of energy supplied to the compressor. The ECS can also regulate the scavenging pressure by modifying the VGT position.

The Exhaust Gas Bypass (EGB) can be used to regulate the scavenging pressure. When the EGB opens part of the exhaust gases bypasses the turbine and the turbine mass flow is reduced. The EGB is also used as a safety feature, because when a EGR shutdown is requested the EGB is opened to avoid undesired accelerations of the turbocharger. In a EGR shutdown the recirculation of gas is suddenly stopped and the turbocharger tends to accelerate due to the increase of the turbine flow. The EGB will not be part of the model proposed in this project.

2.2 Exhaust Gas Recirculation components

The Shut Down Valve (SDV) can only take two positions: open or closed. The purpose of this valve is to control when gases are allowed into the EGR loop. Before introducing the exhaust gas into the scavenge manifold, it needs to be cleaned to avoid corrosion due to the high concentrations of SO_2. The pre-scrubber and the scrubber modules are responsible for the cleaning process. The internal functioning of these components are considered outside of the scope of this project.

The EGR cooler is externally regulated to ensure that the gases recirculated trough the EGR loop have the same temperature as the scavenging manifold independently of the flow. The WMC module removes any the condensed water in the cooling process.

Two EGR blowers are needed to overcome the pressure difference between the manifolds. The two EGR blowers in parallel allow a wider mass flow operational range. In situations where both blowers are running, they do it at the same speed to avoid back flows.

The Change Over Valve (COV) is used for the same purpose as the SDV, but it can take multiple opening positions. The SDV is not modeled since it has the same functionality as the COV, although its correct operation must be verified from the measurements.

The sequence of an EGR start up begins with the recirculation valve opening earlier than the SDV and COV, which allows the EGR blower to build up the needed pressure difference in order to avoid backflow. When the blower is running at the desired speed, then the COV and SDV are opened and the recirculation valve is closed. Evidence of leakages in the recirculation valve were confirmed by MAN engineers during the duration of the tests. Therefore a model of the leakage is included in the EGR model.

When high EGR flows are used, both the exhaust gas temperature and the energy transferred through the turbocharger decrease. To avoid slowing down the turbocharger, part of the compressed air can be recirculated into the turbine inlet to boost the turbocharger. The Cylinder Bypass Valve (CBV) regulates the amount of recirculated fresh air. The usage of CBV is commonly associated to situations when the two EGR blowers are running. The CBV is an important component of the system, but for the sake of simplicity is kept out of the model.

2.3 Data Assessment

2.3.1 Available Datasets

MAN Diesel&Trubo provided the experimental data described in this section. The data corresponds to EGR tests performed in the research center during the years 2012 and 2013. During this time some of the

engine components have changed, for example the turbocharger. Table 2.2 shows all the measurements used in the project.

Measurements	
Symbol	Description
p_{scav}, p_{exh}	Manifold pressures
T_{scav}, T_{exh}	Manifold temperatures
O_{scav}, O_{exh}	Manifold oxygen content
$\dot{m}_{egr}$	Recirculated mass flow
N_{TC}	Turbocharger angular velocity
p_{amb}, T_{amb}, RH_{amb}	Ambient temperature, pressure and relative humidity

Table 2.2: List of measurements used in the derivation and validation of the model

Note that the only mass flow measurement corresponds to the EGR flow. Likewise, undesired noise was observed in the EGR flow signal when the COV was closed, which could be caused by small leaks or an incomplete closing of the COV. Such behaviour is undesired. Since the EGR flows are normally much higher than the noise amplitude, all mass flows lower than $0.6\ kg/s$ are filtered out. A list of the mandatory conditions to be fulfilled in order to consider a dataset follows:

- All input signals should be available, as well as the EGR mass flow, CBV, shutdown requests and auxiliary blower signals.
- The EGB valve must be unused as well as the CBV.
- The Auxiliary blowers must not be activated.
- The turbocharger maps and the EGR blower map must be available.

The only data fulfilling the criteria was logged during experimental tests done in January 2013. In those tests the VGT signal is missing but it was kept at a constant position of 33% in all datasets. The model is created so it is capable to handle multiple VGT positions. The data do not include cases in which the two EGR blowers were running in parallel, since in those situations the CBV is normally opened.

A total of 6 datasets are gathered, most of them are operated at 50% and 75% load. Three datasets are used for model tuning, the remaining are used for model validation. The model inputs are summarized in Table 2.3. The inputs of the model for the tuning datasets are shown in figures 2.2, 2.3 and 2.4. The inputs for the validation datasets can be found in Appendix B.

System inputs	
Symbol	Description
$Load$	Engine control system internal load
ERM	Engine running mode
N_{blow}	EGR blower angular speed
u_{COV}	Change over valve opening percentage

Table 2.3: List of the model inputs

We consider three datasets in the tuning procedure because some of the parameters are tuned depending on load, and these three datasets cover the load range from 25% to 100%. The validation datasets are all operated at load between 50% and 75%, and no validation data are available for load outside this range. The available data is assumed to be representative to tune the model and verify the obtained simulation results.

Dataset 1 contains a load step from 50% to 75% load without EGR. The step is followed by the start up of the EGR system and a sequence of small steps in the EGR blower speed.

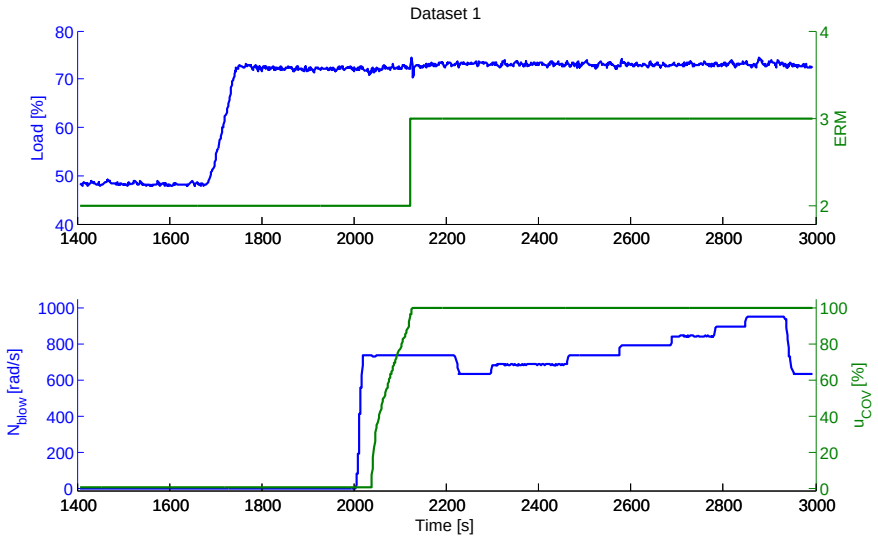

Figure 2.2: Input signals from dataset 1

Dataset 2 shown in Figure 2.3 includes a load step from 25% to 50% load without EGR. The auxiliary blowers are not active during the 25% load, this situation is not possible in normal operation, therefore the scavenge process is expected to be negatively effected. Two tests are present in this dataset, between samples 1900 and 2300 the EGR system is twice intended to start. The first attempt shows both COV and SDV open, the EGR blower is running and the ECS changes to ERM 3 but no mass flow is measured. The reason of such situation is that the EGR flow is manually blocked on purpose to test the alarm system. In the second attempt the COV and the SDV were kept closed, and no mass flow was measured either.

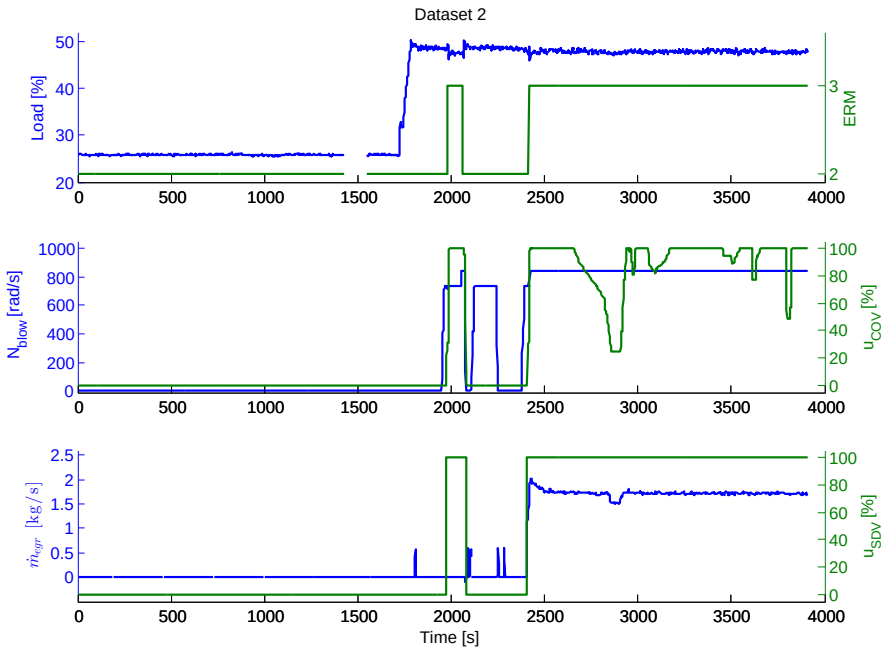

Figure 2.3: Input signals from dataset 2

Dataset 3 shown in Figure 2.4 is the only dataset with loads over 75%. Another interesting feature of this dataset is that load varies from 50% to 100% with a constant EGR blower speed.

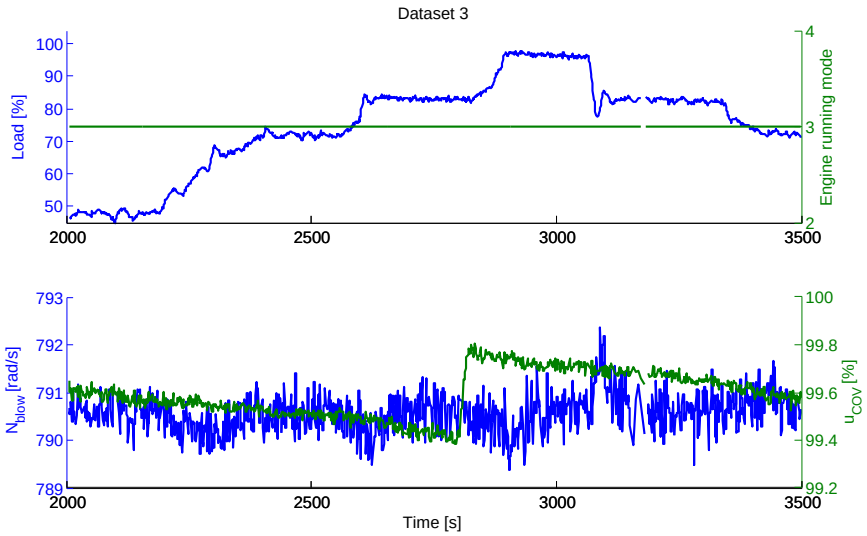

Figure 2.4: Input signals from dataset 3

2.3.2 Oxygen sensors

A Horiba[1] emissions analyzer was placed in the turbine outlet during January 2013, therefore emissions measurements are available in all datasets. The emission analyzer gives a dry volumetric fraction of CO_2, O_2, NO_x and CO. A dry measurement means that the water content is removed before measuring the species content. Consequently a dry volumetric fraction of an specie is always higher than the wet volumetric fraction. The Horiba equipment datasheet specifies a response time of $3.5s$.

The scavenge manifold oxygen measurement is also a volumetric fraction but in this case it corresponds to a wet measurement. A measurement delay substantially larger than the Horiba sensor is observed, which can be explained by the long pipes between the sensor and the receiver.

A small bias in the scavenging oxygen content is observed when the EGR system is not active. If no exhaust gas is recirculated, the oxygen content in the scavenge manifold should correspond to 20.95%, which is the volumetric percentage of oxygen in the atmosphere. Figure 2.5 shows the interval [1100:2200][s] of dataset 2 where EGR was not used. A bias is observed in the scavenging oxygen content as well as a pressure dependency, which is explained by the increase of the sensor flow due to an increase in scavenge pressure.

2.3.3 Re-sampling

A marine engine is a highly complex system with multiple distributed control units and data acquisition units. The Engine Diagnostics System (EDS) is the system in charge of logging all the data from the different units. The sampling frequency is not constant, as it depends on the response time of the slowest unit. If one unit is unresponsive, the last known value is logged. It is also observed that some signals have lower resolution than others depending on the unit sensing them.

[1] A japanese manufacturer of precision instruments for measurement and analysis of emission gases

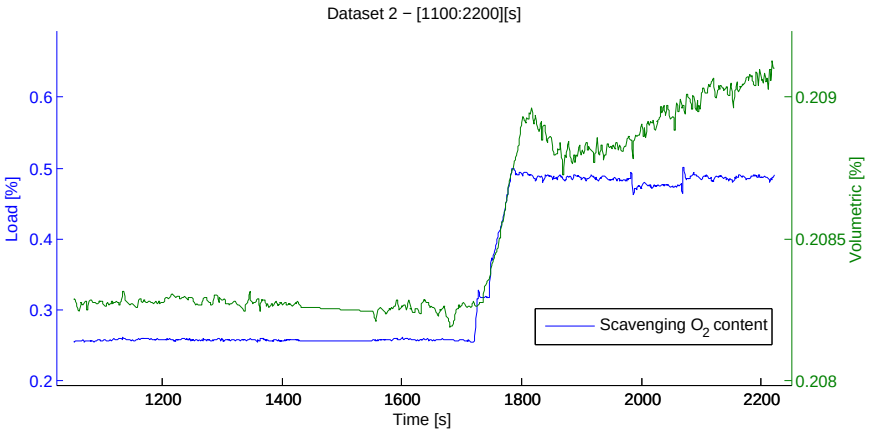

Figure 2.5: Measured O_2 volumetric fraction in scavenge manifold

To overcome the variable sampling frequency the signals are re-sampled to a common and constant sampling frequency of $1\ Hz$. The measurements sampling frequency varies between $1.1\ Hz$ and $0.8\ Hz$.

Different signal resolutions are noticed between p_{exh} and p_{scav}. The ECS rely on p_{scav} to determine the compression ratio, which explains why p_{scav} has a higher resolution than p_{exh}. The pressure ratio over the engine is defined by both signals, having different pressure resolutions implied having a pressure ratio with sudden and abrupt changes. This fact motivated the modification of the measured signals. Such modification consists of selecting the relevant samples and performing a linear regression between them. A relevant sample is defined as being different from its previous sample. When a maximum or a minimum is found, both the initial and final samples are considered relevant. Such modification of the signal is only applied to measured signals, those generated by the ECS are not changed. Figure 2.6 shows an example of how a measured signal is modified compared to the original signal.

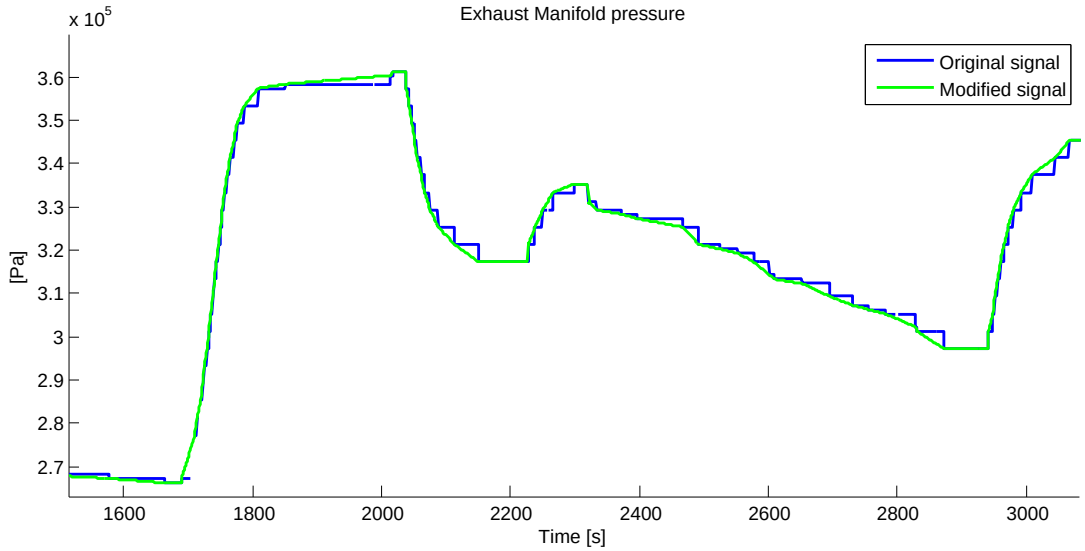

Figure 2.6: Example of the re-sampling result

CHAPTER 3

Thermodynamic MVEM

A Mean Value Engine Model (MVEM) is presented in this chapter. The simulation environment chosen is Simulink[1] due to previous modeling work targeting the same engine (Pedersen 2013) and (Mahler 2013). The main difference compared to the previous projects is that the aim of the proposed model is not to design a controller for the EGR system, but to evaluate the performance of EGR controllers.

The different components conforming the model are enumerated here:

1. Turbocharger
2. Cylinder
3. Scavenge and exhaust manifolds
4. EGR system

From the end user point of view the final model inputs and output are shown in 3.1. The model inputs are the ECS internal load, the VGT and COV opening percentages and the EGR blower speed (N_{TC}). The signal $Engine\ Running\ Mode$ (ERM) indicates in which mode the ECS is regulating the engine. The set points for the opening and closing of the exhaust valve depend on the running mode.

The output of the model is the oxygen content in the scavenging manifold. The aim of the EGR system is to reduce the formation of NO_x by reducing the amount of oxygen available for the combustion, therefore O_{scav} represents a good performance indicator.

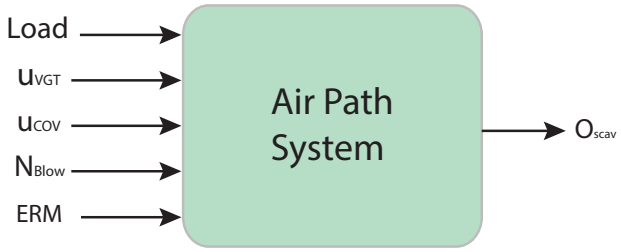

Figure 3.1: Model inputs and output

For simplification purposes, the externally regulated modules presented in the previous chapter (both cooling units with their respective WMCs, the preheater unit, the pre-scrubber and the Scrubber) are not considered in the model. The assumptions taken from those simplifications are listed here:

[1] Simulink is a block diagram environment for multidomain simulation and Model-Based Design(Math-Works n.d.)

- The preheater ensures a constant temperature of $25^{\circ}C$ in the compressor inlet.
- The pressure drops in Preheater, AC, WMC, Prescruber, scrubber, EGR cooler and pipes are not considered.
- The temperature of the scavenging manifold is assumed constant since both cooling units have this goal. The temperature increase from the EGR blower is considered neglectable.
- The composition of the exhaust gas passing through EGR is assumed unchanged.
- Variations of the spacial distribution of species inside the manifolds are neglected. Instantaneous and ideal mixing is assumed in all control volumes.

3.1 Turbo Charger

The turbocharger is a critical component in the model because it defines the incoming and outgoing mass flows of the system and none of them are available for validation. The turbocharger is the first component modeled since the other components depend on these mass flows. The performance characteristics of both the compressor and the turbine are provided by MAN in a form of a tabulated performance map.

Figure 3.2 shows the inputs and outputs of the turbocharger submodel. The ambient conditions p_{amb} and T_{amb} are assumed constant as well as the scavenging temperature T_{scav}. Both manifold pressures p_{scav} and p_{exh} as well as the exhaust temperature T_{exh} are inputs, the position of the variable geometry turbine is included as an input although it is kept constant in all datasets. The Air-fuel ratio is the air mass flow divided by the fuel mass flow, it is needed to define the composition of the turbine mass flow gas. The outputs of the turbocharger block are both the compressor and the turbine mass flows.

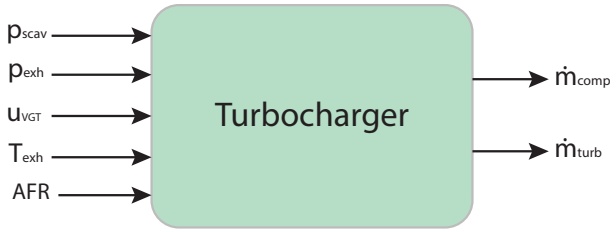

Figure 3.2: Inputs and outputs of the turbocharger block

Previous modeling worked done with the same turbocharger (Tao 2012), (Mahler 2013) and (Pedersen 2013) used polynomial fitting to model the performance maps. The highly non-linear performance maps were fitted using two dimensional forth order polynomials for both mass flows, as well as the efficiencies.

Three possible modeling options were considered. The first option was to select only the areas of the performance map where the turbocharger is commonly used, and perform a similar polynomial fitting as in previous work. The second option was to use superellipses to describe the relation between the dimensionless parameters, as done in (Eriksson 2007). The third option was to model the turbocharger with an advance simulation software and couple it with the Simulink model. Engineers at MAN are using GT-Power[2] for steady state simulations, which is an industry standard in terms of engine simulator software. This software is thought to suit the needs since it is also meant for dynamic simulations and has the possibility to be coupled with Simulink.

The third option is considered to be the most suitable in that phase of the project. Externalizing the model of the turbocharger to a high fidelity simulator allows the validation of the remaining components

[2]GT-Power is part of GT-Suite Software (Gamma-Technologies n.d.)

with reliable mass flows. This option was thought to be an intermediate step before using one of the other modeling options, but due to the duration of the Master thesis the other options have not been pursued further. In section 3.1.2 an explanation of the coupling between the Simulink environment and the GT-Power environment is given.

3.1.1 Turbine and Compressor maps

Both the compressor and Turbine performance maps are based on the Society of Automotive Engineers standards (SAE-J922 2011) and (SAE-J1826 1995). These standards specify the conditions and equipment needed to create the maps in order to compare turbochargers with different characteristics. An SAE map consists on a series performance data points organized in groups at fixed speeds . Each point describes an operating condition in terms of speed, pressure ratio, mass flow rate, and thermodynamic efficiency.

The SAE maps are typically supplied in a modified format to take into account the changes in temperature, pressure and composition of the gas. In this case the modifications differs for a compressor and a turbine map. A turbine map is normally reduced with the transformation shown in equation 3.1.

$$N_{reduced} = \frac{N_{actual}}{\sqrt{T_{inlet}}} \qquad \dot{m}_{reduced} = \frac{\dot{m}_{actual}\sqrt{T_{inlet-total}}}{p_{inlet-total}} \tag{3.1}$$

where N_{actual} corresponds to the measured turbocharger speed in $[RPM]$, the T_{inlet} corresponds to the turbine inlet temperature in $[K]$ and the $p_{inlet-total}$ is the total pressure at the inlet of the turbine in $[Pa]$. The total pressure is defined as the sum of the static and the dynamic pressures.

The compressor maps are typically corrected to a reference inlet temperature and pressure. The correction transformation is shown in equation 3.2.

$$N_{corrected} = \frac{N_{actual}}{\sqrt{\frac{T_{inlet}}{T_{ref}}}} \qquad \dot{m}_{corrected} = \frac{\dot{m}_{actual}\sqrt{\frac{T_{inlet}}{T_{ref}}}}{\frac{p_{inlet-total}}{p_{ref}}} \tag{3.2}$$

where the reference pressure p_{ref} corresponds to $10^5\ Pa$ and the reference temperature T_{ref} to $298\ K$ as the SAE standard J922 specifies.

The turbine is equipped with a nozzle ring capable to modify the inlet area, different map are needed to characterize different inlet areas. MAN Diesel&Turbo provided ten maps corresponding to ten areas, the maximum and minimum areas are found in the turbine characteristics datasheet. Linear interpolation is applied to calculate the VGT opening percentages u_{VGT} for each of the available maps, as seen in Equation 3.3.

$$u_{VGT_i}[\%] = \frac{A_i - A_{min}}{A_{max} - A_{min}} \tag{3.3}$$

where A_{min} and A_{max} corresponds to the minimum and maximum inlet area of the ring. The A_i is the area on a specific map i. All the maps with their respective u_{VGT} are used in the GT-Power model.

3.1.2 GT-Power simulator coupled with Simulink

The GT-Power model of the turbocharger is kept as simple as possible. The idea behind the model is to characterize both the inlet and the outlet of the turbine and compressor from Simulink. The characterization of the gas requires: the temperature, the pressure and the gas composition. Figure 3.3 shows the overview of the GT-Power model. The fuel and air fraction is sent to GT-Power to to modify the composition of the gas driving the turbine.

The GT-Power software comes with a Simulink block which makes the coupling easier. The block is capable to managing the interaction between the two solvers if they run at different integration steps. Since the GT-Power solver must run at a fixed step it becomes the bottleneck of the simulation in terms of time. The Simulink part can run at a fixed or at a variable step. For simplicity both solvers are set to an explicit Runge-Kutta method, which is the GT-Power solver recommended by MAN engineers. In section 6.3 a comparison of simulation time for the different Simulink solvers is carried.

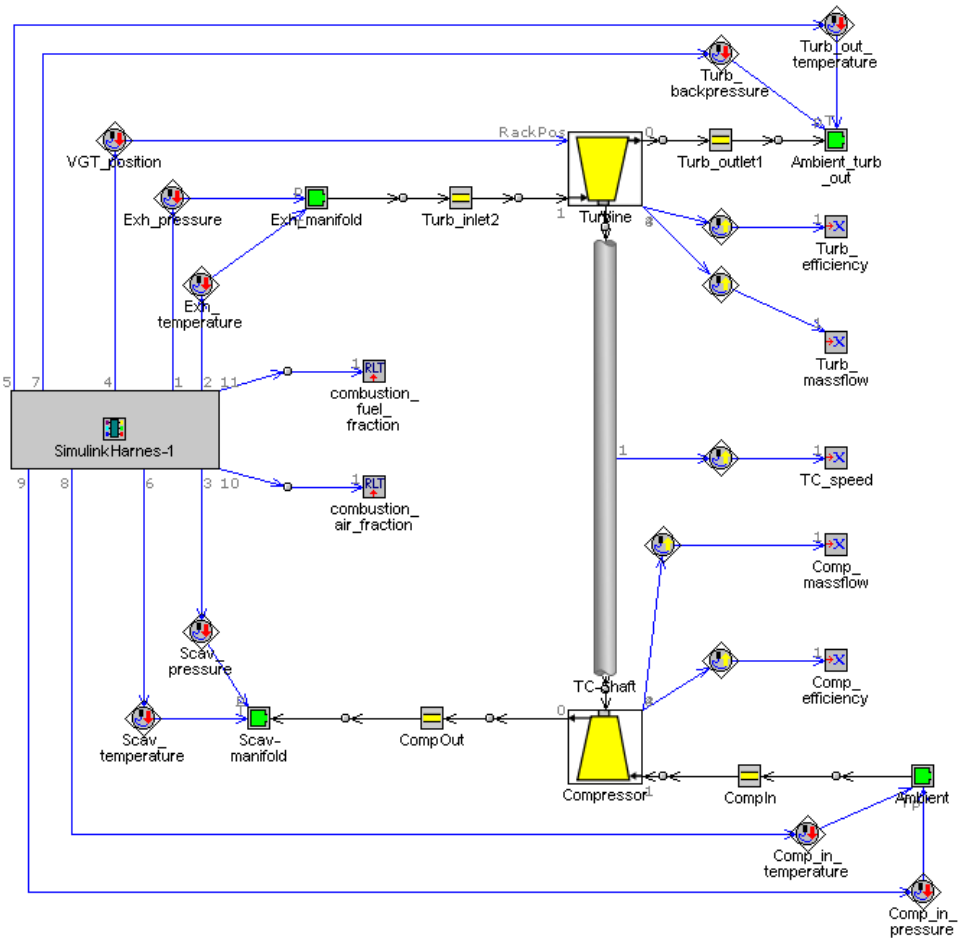

Figure 3.3: Turbocharger model implemented in GT-Power

With the purpose of designing the model as generic as possible u_{VGT}, $p_{comp_{in}}$, $T_{comp_{in}}$ and $p_{turb_{out}}$ are modeled as dynamic signals even if they are assumed to be constant. Both $p_{comp_{in}}$ and $p_{turb_{out}}$ are assumed to be the atmospheric pressure. The outlets temperatures of the compressor and turbine are unknown and need to be estimated. The output of the model are the mass flows, the turbocharger speed for validation purposes and the turbine and compressor efficiencies which are used to estimate the outlet temperatures.

Equation 3.4 can be derived from the definition of the compressor efficiency as explained in (Watson and Janota 1982).

$$T_{comp_{out}} = T_{comp_{in}} \left(1 + \frac{\left(\frac{p_{scav}}{p_{amb}} \right)^{\frac{\gamma_{air}-1}{\gamma_{air}}} - 1}{\eta_{comp}} \right) \tag{3.4}$$

where η_{comp} is the compressor efficiency, (p_{scav}/p_{amb}) is the compressor pressure ratio and γ_{air} corresponds

to the heat capacity ratio of air.

The temperature in the turbine outlet is also derived from the turbine efficiency definition. Equation 3.4 and 3.5 are modeled in Simulink and both temperatures are fed back to GT-Power.

$$T_{turb_{out}} = T_{turb_{in}} \left(1 - \eta_{turb} \left(1 - \left(\frac{p_{amb}}{p_{exh}} \right)^{\frac{\gamma_{exh}-1}{\gamma_{exh}}} \right) \right) \tag{3.5}$$

where η_{turb} is the turbine efficiency, (p_{amb}/p_{exh}) is the turbine pressure ratio and γ_{exh} corresponds to the heat capacity ratio of the exhaust gas.

The block inputs are the signals that are sent to the GT-power simulation, while the block also allows to modify any parameter used in the GT-power model, e.g. the composition of fuel. The reason for not specifying the parameters inside GT-power is to have the capability to change all the simulation parameters from Simulink. A list of the parameters in the GT-Power model follows.

1. The pipe diameters
2. The composition of Air
3. The number of carbon and hydrogen in a molecule of fuel.
4. The Low Heating Value (LHV) of fuel.
5. The turbocharger inertia
6. Initial conditions for each of the signals.
7. Discretization length in the pipes, important for the internal solver.

For further information on the coupling possibilities refer to *Controls Coupling Manual* available with GT-Suite Software (Gamma-Technologies n.d.).

3.2 Cylinder

In this section a model of the cylinders is derived. All four cylinders are treated as only one. The outputs of the cylinder block are the intake mass flow $\dot{m}_{del}$ and outgoing mass flow $\dot{m}_{eng_{out}}$, the remaining oxygen after the combustion $O_{eng_{out}}$ and the temperature of the outgoing gases T_{cycle} and depicted in Figure 3.4.

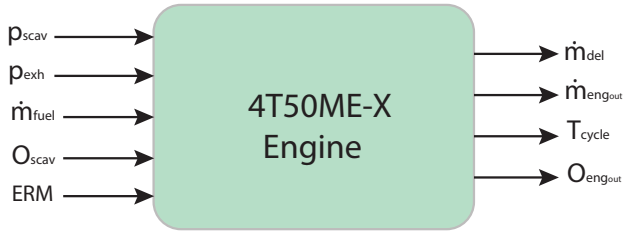

Figure 3.4: Inputs and outputs of the cylinder block

Figure 3.5 shows the cyclic processes of a 2-stroke engine as a function of the crank angle. The Top Dead Center (TDC) corresponds to the highest piston position in the stroke, and the Bottom Dead Center (BDC) to the lowest piston position. The Exhaust Valve Opening (EVO) and the Exhaust Valve Closing (EVC) are regulated by the ECS, therefore are represented with a span of possible angles. The angles defining the

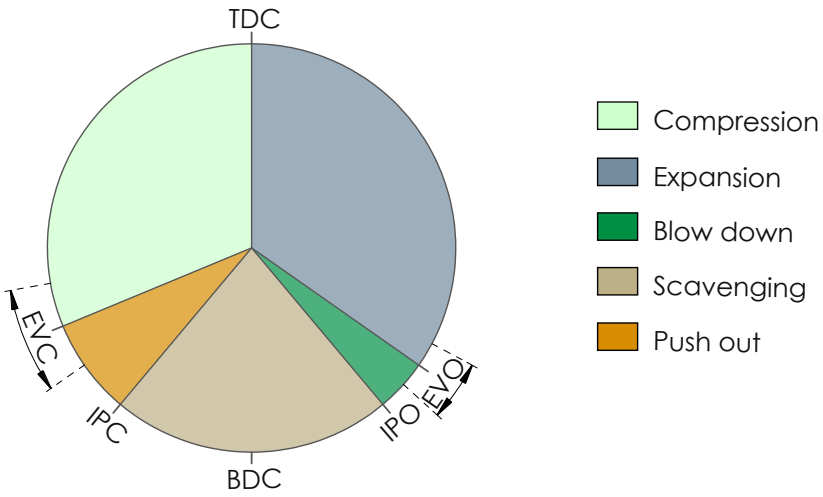

Figure 3.5: 2-Stroke cycle processes

intake ports opening (IPO) and intake ports closing (IPC) are dependent on the port geometry, the stroke and the connecting rod length.

During the Blowdown process the combustion products are flushed due to the pressure difference between the cylinder and the exhaust manifold. The ECS regulates the pressure at IPO by modifying the EVO angle, thus avoiding any backflow. The scavenging process removes the remaining combustion products with fresh charge. During the Post-scavenging process the piston is moving towards the TDC, pushing the gas in the cylinder to the exhaust manifold. The EVC angle is varied to regulate the compression ratio. The IPO and the IPC are 140º and -140º respectively from TDC.

The evaluation the scavenging process in a 2-Stroke engine is commonly assessed with the parameters 3.6 and 3.7. Their definition can be found in (Heywood 1988) and Rajput (2005).

$$\text{Scavenging efficiency} = \frac{\text{Mass of delivered air retained}}{\text{Mass of trapped charge}} \tag{3.6}$$

$$\text{Trapping efficiency} = \frac{\text{Mass of delivered air retained}}{\text{Mass of delivered air}} \tag{3.7}$$

As mentioned previously, the considered engine employs an uniflow scavenging method which has a high scavenging efficiency. In section 4.3 the considered ranges of both efficiencies are explained.

3.2.1 Engine outgoing mass flow

Conservation of mass describes the outgoing mass flow as the sum of the two incoming mass flows on the engine block, i.e.,

$$\dot{m}_{eng_{out}} = \dot{m}_{del} + \dot{m}_{fuel} \tag{3.8}$$

where $\dot{m}_{eng_{out}}$ is the mass flow entering the exhaust manifold, the $\dot{m}_{del}$ corresponds to the delivered mass flow during the scavenging process and the $\dot{m}_{fuel}$ is the fuel mass flow.

3.2.2 Engine inlet mass flow

In 4-stroke engines, the mass flow trough the engine is commonly modeled with the volumetric efficiency (Vigild 2001), (Wahlström and Eriksson 2011) and Heywood (1988). For 2-stroke engines a different approach is needed.

The mass flow $\dot{m}_{del}$ passing through the engine can be approximated as an incompressible flow through a restriction with equation 3.9. This modeling approach is also used in (Hansen et al. 2013) and (Wahlström and Eriksson 2011). The incompressible assumption is valid since the scavenging process is substantially below the speed of sound. The continuous flow through the restriction represents the overall mass flow of all cylinders.

$$\dot{m}_{del} = A_{eng} \frac{p_{scav}}{\sqrt{R_{scav} T_{scav}}} \sqrt{\frac{2\gamma_{scav}}{\gamma_{scav} - 1} \left(\frac{p_{scav}}{p_{exh}}^{\frac{2}{\gamma_{scav}}} - \frac{p_{scav}}{p_{exh}}^{\frac{\gamma_{scav}+1}{\gamma_{scav}}} \right)} \tag{3.9}$$

where R_{scav} is the specific gas constant, A_{eng} corresponds to the cross sectional area of the orifice. In this project A_{eng} is considered constant although the mass flow through each cylinder is not constant. The pulsation effects due to the different cylinders timing are considered neglectable because the time constants of the system are substantially larger than the pulsations frequency.

3.2.3 Oxygen burned in the combustion

The oxygen fraction of the cylinder outgoing mass flow is described in equation 3.10, which is based upon mass conservation and the oxygen mass fractions of the incoming and outgoing mass flow. The same modeling approach is found in (Wahlström and Eriksson 2011) and (Hansen et al. 2013), although a gain factor is introduced due to the inconsistency of the simulation results with the measured O_{exh}. In (Mahler 2013) these gain factor was introduced to overcome the same inconsistency. This model inconsistency with respect to the measurements could be caused by a leak in the cylinder bypass valve, because it would induce the Horiba analyzer to measure a higher oxygen measurement, although it has not been proven in this project.

The oxygen consumed in the combustion is subtracted from the oxygen present in the delivered mass flow. This is equivalent to subtract the oxygen consumed in the combustion from the trapped mass flow and keep O_{scav} for the mass flow which is not trapped. All fuel injected is assumed to react, hence the combustion is considered to be complete and ideal.

$$O_{eng_{out}} = \frac{K_{Oscav}\, \dot{m}_{del}\, O_{scav} - \dot{m}_{fuel}\ (A2F)_s\ O_{amb}}{\dot{m}_{eng_{out}}} \tag{3.10}$$

where the air to fuel ratio $(A2F)_s$ corresponds to the kg of air needed to burn $1\ [kg]$ of fuel, the sub-index s indicates that it is based on the stoichiometric combustion. O_{amb} is the oxygen mass fraction in atmospheric air, it is used to convert the air-fuel ratio to oxygen-fuel ratio. The tuning gain factor is K_{Oscav}.

Equation 3.11 shows the stoichiometric combustion for a generic fuel composed of only carbon and hydrogen from (Heywood 1988). This simplified combustion model assumes that the molecular structure of fuel does not have oxygen. It also assumes that HC, CO and NO_X formation are neglected.

$$\begin{aligned} CH_y + (1 + 0.25y)\,(O_2 + r_{N_2} N_2 + r_{Ar} Ar + r_{CO_2} CO_2) \ \rightarrow \\ (1 + r_{CO_2}\,(1 + 0.25y))\, CO_2 + (0.5y)\, H_2O + (1 + 0.25y)\,(r_{N_2} N_2 + r_{Ar} Ar) \end{aligned} \tag{3.11}$$

Parameters r_i are the molar ratios of the elements with respect to one oxygen mole in the atmosphere. The reaction have been scaled to one carbon molecule because the molecular structure of the fuel is unknown. The molar relation between carbon and hydrogen y can be obtained from the fuel properties.

The air to fuel stoichiometric ratio can be calculated using equation 3.12. The molar weights (MW) of air, C and H are needed to be able to express the ratio in mass basis.

$$(A2F)_s = (1 + 0.25y)\ \frac{(1\,O_2 + r_{N_2}N_2 + r_{Ar}Ar + r_{CO_2}CO_2)\,MW_{air}}{MW_C + y\,MW_H} \tag{3.12}$$

The molar weight of a mixture, in this case air, is calculated as shown in equation 3.13.

$$MW_{mix} = \sum_i x_i\,MW_i \tag{3.13}$$

A reliable measurement of the fuel mass flow $\dot{m}_{fuel}$ is essential to estimate the amount of oxygen needed to burn all the fuel. MAN engineers advised that the measured fuel mass flow is not a reliable measurement, therefore the amount of fuel injected in all cylinders is considered to be proportional to the ECS internal load.

It has been possible to gather over 70 performance analysis carried during the year 2013. A performance analysis is a report with all engine measurements averaged over 5 minutes. Previous to carrying a performance analysis, the engine operation is not changed for 20 minutes to ensure a thermal stability.

In all performance analysis reports, two different measurements of fuel consumption are available. The maximum measurement error is known to be $\pm 2\,\%$ of the measured value. Figure 3.6 shows the fuel mass flow versus the load from all the performance analysis. The linear regression obtained is used to describe $\dot{m}_{fuel}$ as a function of load, the regression results are shown in equation 3.14.

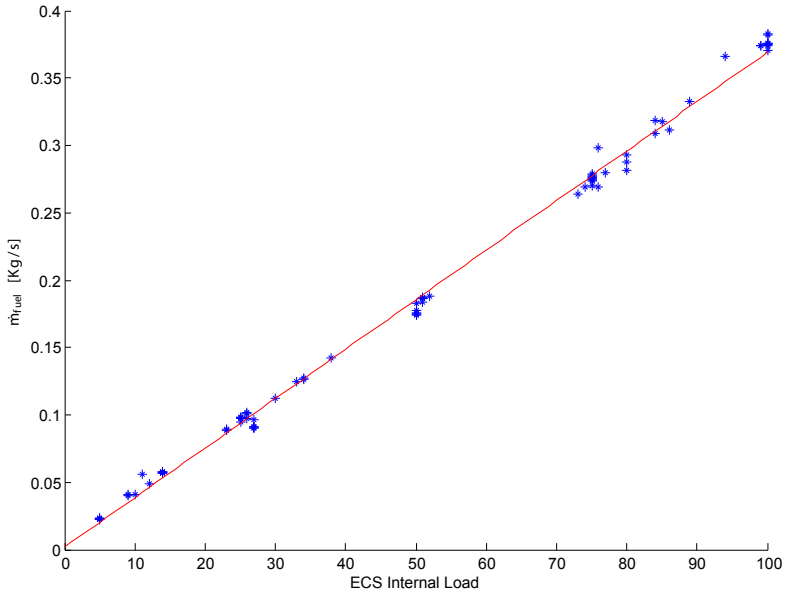

Figure 3.6: $\dot{m}_{fuel}$ as a function of Internal Load

$$\dot{m}_{fuel} = 0.00367 * Load\,[\%] + 0.00187 \qquad R^2 = 99.658\% \tag{3.14}$$

3.2.4 Engine outlet mass flow temperature

The temperature of the engine outgoing mass flow is estimated using the Seiliger cycle approximation. An advantage for using a Seiliger cycle compared to a Diesel cycle is the capability to replicate the two

phases of the combustion. The premixed combustion phase corresponds to the combustion at constant volume, and the mixing controlled combustion corresponds to the heat addition at constant pressure.

The Seiliger cycle approximation has been used with the same purpose in (Skogtjärn 2002) and (Wahlström and Eriksson 2011). A more advanced Seiliger cycle is presented in Byungchan Lee and van Nieuwstadt (2013). But in all of those cases the Seiliger cycle was based on a 4-stroke engine. The Seiliger cycle in this project follows the same methodology as (Skogtjärn 2002) with some modifications in order to be consistent with the 2-stroke closed cycle. Figure 3.7 shows the in-cylinder pressure versus cylinder relative volume diagram corresponding to a 2-stroke engine.

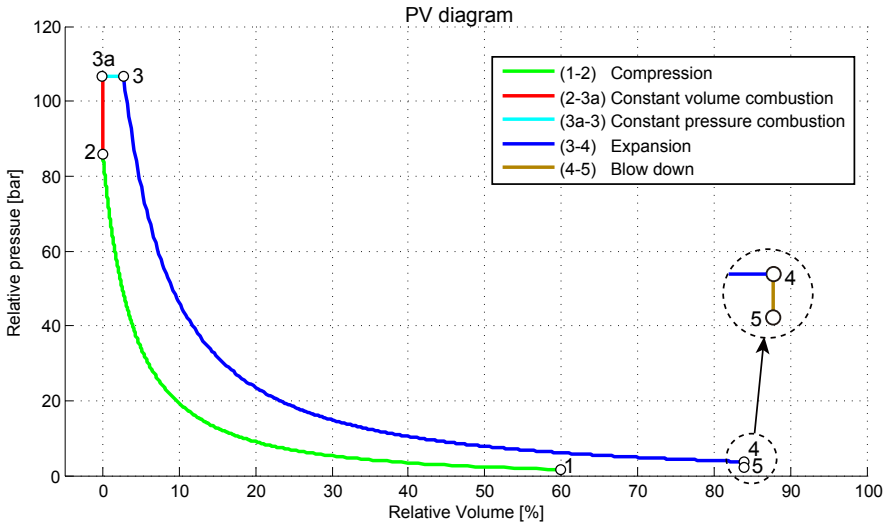

Figure 3.7: Seiliger cycle diagram corresponding to a 2-Stroke engine

Points 1,2,4 and 5 correspond to EVC, TDC, EVO and IPO respectively. The pressure at points 1 and 5 is assumed to be equal to the exhaust pressure. At IPO no backflow is considered since the cylinder pressure is supposed to be lower than the scavenging pressure during the blowdown process.

The pressure and temperature at the end of the constant volume combustion are described by equations 3.15. The temperature at the end of the second phase of the combustion at constant pressure is described by equation 3.16.

$$p_{3a} = p_2 \left(1 + \frac{q_{in}}{c_{v_{scav}} T_2}\right) x_{cv} \qquad T_{3a} = T_2 + \frac{q_{in}}{c_{v_{scav}}} x_{cv} \tag{3.15}$$

where q_{in} corresponds to the specific energy content of the charge, x_{cv} corresponds to the ratio of fuel burned at constant volume and $c_{v_{scav}}$ is the constant volume heat capacity of the scavenging gas.

$$T_3 = T_{3a} \frac{v_3}{v_{3a}} = T_{3a} + \frac{q_{in}}{c_{p_{scav}}} (1 - x_{cv}) \tag{3.16}$$

where V_{3a} corresponds to the compression volume and $c_{p_{scav}}$ is the constant pressure heat capacity of the scavenging gas.

During the compression and the expansion heat transfer with the cylinder walls is considered. This phenomenon is omitted in the formulation presented in (Skogtjärn 2002) since both processes are considered adiabatic. But the heat transfer is important to be considered for the 4T50ME-X because, compared to a heavy duty 4-stroke engine, the cycle time is considerably longer. Therefore, more time for the heat exchange is available.

The compression and the expansion processes can be described by a polytropic process which obeys the law 3.17. The two equities P-V relation and T-V relation are equivalent.

$$P\,V^n = Constant \qquad\qquad T\,V^{n-1} = Constant \tag{3.17}$$

where n corresponds to the polytropic coefficient. If the process is considered adiabatic n corresponds to the gas heat capacity ratio γ_{gas}. If heat is added during the process, then the value of n is higher than the γ_{gas}. On the other hand if heat is dissipated in the process a n smaller than γ_{gas} is expected. During the expansion process heat is expected to be dissipated and during the compression the cylinder walls are expected to provide heat to the process. The blowdown process is assumed to obey an adiabatic expansion process due to its short duration.

An expression of the temperature at the end of the blowdown process $T_5 = T_{cycle}$ can be obtained rearranging equations 3.15, 3.16 and 3.17. The resulting expression is shown in equation 3.18.

$$T_{cycle} = \left(\frac{V_1}{V_2}\right)^{1-\gamma_{comp}} \left(\frac{V_3}{V_4}\right)^{\frac{\gamma_{exp}}{\gamma_{scav}}-1} x_p^{1/\gamma_{scav}-1} \left(q_{in}\left(\frac{1-x_{cv}}{c_{p_{scav}}} + \frac{x_{cv}}{c_{v_{scav}}}\right) + T_1\,\left(\frac{V_1}{V_2}\right)^{\gamma_{comp}-1}\right) \tag{3.18}$$

where γ_{comp} and γ_{exp} are the polytropic coefficients for the compression and the expansion respectively. The volumes V_1 and V_4 are variable and their characterization from the ECS internal parameters is explained in section 4.3. V_2 corresponds to the compression volume. x_p is the pressure ratio between the points 2-3 and is described by equation 3.19. The specific energy content of the charge q_{in} is described by equation 3.20. The volume at the start of the expansion V_3 is described by equation 3.21. The temperature at the beginning of the closed cycle T_1 is estimated in equation 3.22.

$$x_p = \frac{p_3}{p_2} = 1 + \frac{q_{in}x_{cv}}{c_{v_{scav}}T_1\left(\frac{V_1}{V_2}\right)^{\gamma_{comp}-1}} \tag{3.19}$$

$$q_{in} = \frac{\dot{m}_{fuel}\,LHV}{\dot{m}_{trap}+\dot{m}_{fuel}}\eta_{scav} \tag{3.20}$$

$$V_3 = V_2\left(1 + \frac{\frac{q_{in}}{c_{p_{scav}}}(1-x_{cv})}{T_1\left(\frac{V_1}{V_2}\right)^{\gamma_{comp}-1} + \frac{q_{in}}{c_{v_{scav}}}x_{cv}}\right) \tag{3.21}$$

$$T_1 = (1-\eta_{scav})\,T_{cycle} + \eta_{scav}T_{scav} \tag{3.22}$$

where $\dot{m}_{trap}$ corresponds to the engine intake mass flow multiplied by the trapping efficiency. The LHV corresponds to the Low Heating Value of the fuel. The η_{scav} corresponds to the scavenging efficiency 3.6 and it is used to describe the residual gas ratio of the charge.

3.3 Manifolds

The manifolds are modeled as dynamic control volumes. A control volume is a unique mathematical point representing the mean value of a three dimensional complex object. To describe this control volume the temperature, pressure and oxygen content are taken into account. The oxygen content in the control volume is defined as the mass of oxygen divided by the total mass of the gas.

3.3.1 Scavenge air manifold

The scavenge manifold has only two internal states, the pressure p_{scav} and the oxygen content O_{scav}. The temperature is assumed constant and therefore all incoming flows have the same constant temperature. The inputs of the model are shown in Figure 3.8.

Figure 3.8: Inputs and outputs of the scavenge manifold block

The scavenge manifold is modeled as an isothermal control volume, which assumes a constant temperature throughout all the control volume. The energy equilibrium is violated with this approximation, but such simple and compact representation of the control volume dynamics fits perfectly with the assumption of a constant T_{scav}.

Pressure

Equation 3.23 is obtained from deriving the ideal-gas law and applying mass conservation to describe the derivative of mass. The same modeling approach is found in (Heywood 1988), (Wahlström and Eriksson 2011) and (Hansen et al. 2013).

$$\frac{d}{dt}p_{scav} = \frac{R_{scav}T_{scav}}{V_{scav}}\left(\dot{m}_{comp} + \dot{m}_{egr} - \dot{m}_{del}\right) \tag{3.23}$$

where R_{scav} is the scavenging gas specific constant, V_{scav} is the scavenging manifold volume. The $\dot{m}_{comp}$, $\dot{m}_{egr}$ and $\dot{m}_{del}$ correspond to the compressor mass flow, the recirculated mass flow and the delivered mass flow respectively.

Oxygen content

The manifold oxygen content is driven by a first order differential equation obtained with the same procedure as shown in (Vigild 2001). But for this model the oxygen content is derived instead of the burned fraction. The resulting equation is only affected by the incoming flows and their O_2 content as seen in equation 3.24.

$$\frac{d}{dt}O_{scav} = \frac{R_{scav}T_{scav}}{p_{scav}V_{scav}}\left(\left(O_{exh} - O_{scav}\right)\dot{m}_{egr} + \left(O_{amb} - O_{scav}\right)\dot{m}_{comp}\right) \tag{3.24}$$

The measured oxygen content in the scavenging manifold is a volumetric measurement. To compare the model state O_{scav} with the measured content, the mass fraction needs to be transformed to a molar fraction.

A time lag is observed between the estimated and the measured $O_{scav,meas}$. A measurement delay in O_{scav} is proposed, as shown in equation 3.25. The magnitude of the delay is tuned with measured data in chapter 5.

$$O_{scav,meas}\left(t\right) = O_{scav}\left(t + \tau_{O_{scav}}\right) \tag{3.25}$$

where $O_{scav,meas}$ is the measured oxygen content in the scavenge manifold and $\tau_{O_{scav}}$ is the measurement delay introduced.

3.3.2 Exhaust manifold

The exhaust manifold has three internal states pressure p_{exh}, temperature T_{exh} and the oxygen content O_{exh}. The inputs of the model are shown in 3.9.

Figure 3.9: Inputs and outputs of the exhaust manifold block

The exhaust manifold is modeled as an adiabatic control volume. The adiabatic approximation considers a varying temperature, which depends on the incoming and outgoing mass flows with the correspondent temperatures. The reason to take an adiabatic approximation is to consider two incoming flows with different temperatures. If the trapping efficiency shown in equation 3.7 is lower than 1, it means that some fraction of the delivered gas is not trapped into the cylinder and goes directly to the exhaust. It is assumed that the gas which is not trapped reaches the exhaust manifold with the scavenging manifold temperature.

Pressure

Equation 3.26 describing the exhaust pressure is obtained from the ideal-gas law as in the isothermal approximation, but in this case the temperature derivative is not zero. The same approximation is used in (Vigild 2001) and (Wahlström and Eriksson 2011).

$$\frac{d}{dt}p_{exh} = \frac{R_{exh}T_{exh}}{V_{exh}}\left(\dot{m}_{eng_{out}} - \dot{m}_{egr} - \dot{m}_{turb}\right) + \frac{p_{exh}}{T_{exh}}\frac{d}{dt}T_{exh} \tag{3.26}$$

where R_{exh} is the exhaust gas mixture specific constant, V_{exh} is the exhaust manifold volume.

Temperature

The equation describing the temperature of a control volume is based upon energy conservation. The derivative of the internal energy is driven by the difference between the incoming and outgoing enthalpy ($\dot{H}$) and mass flows, assuming no heat transmission through the walls. The same approach is found in (Guzzella and Onder 2010) and (Eriksson 2007).

$$\begin{aligned}
\frac{d}{dt}T_{exh} &= \frac{R_{exh}T_{exh}}{V_{exh}c_{v,exh}p_{exh}}\left(\dot{H}_{in} - \dot{H}_{out} - c_{v,exh}T_{exh}\left(\dot{m}_{eng_{out}} - \dot{m}_{egr} - \dot{m}_{turb}\right)\right) \\
\dot{H}_{in} &= c_{p,scav}\left(\dot{m}_{del} - \dot{m}_{trap}\right)T_{scav} + c_{p,exh}\left(\dot{m}_{trap} + \dot{m}_{fuel}\right)T_{cycle} \\
\dot{H}_{out} &= c_{p,exh}\left(\dot{m}_{egr} + \dot{m}_{turb}\right)T_{exh}
\end{aligned} \tag{3.27}$$

where $\dot{m}_{del}$ is the delivered mass flow during the scavenging process and $\dot{m}_{trap}$ is the faction of the delivered charge that is trapped in the cylinder. The trapping efficiency defines the relation between the two mass flows.

Oxygen content

The oxygen content in the exhaust manifold is defined with the same approach as the scavenging manifold. The incoming flow is the sum of the delivered flow plus the fuel mass flow. The oxygen content $O_{eng_{out}}$ is the remaining oxygen from the combustion 3.10.

$$\frac{d}{dt}O_{exh} = \frac{R_{exh}T_{exh}}{p_{exh}V_{exh}}\left(O_{eng_{out}} - O_{exh}\right) \tag{3.28}$$

where R_{exh} is the specific gas constant of the exhaust gas, and V_{exh} is the exhaust manifold volume.

The oxygen content is measured at the turbine outlet. Since there are no other incoming flows it is assumed to measure the same concentration as the manifold. The model concentration needs to be transformed from a mass basis to a molar basis in order to compare it with the measurements.

Since the Horiba senses dry measurement, the water content of the gas is needed to perform the transformation from a wet into a dry measurement, as shown in Equation 3.29. A measurement delay of 3.5 s is applied to the estimated O_{exh} as specified in the Horiba datasheet.

$$O_{dry} = \frac{O_{wet}}{(1 - X_{H_2O})} \tag{3.29}$$

where X_{H_2O} is the mass fraction of water present in the exhaust gas.

3.4 EGR loop

The EGR module is the only block that can be decoupled from the air-path model because its unique output is measured. The EGR block includes one EGR blower, the COV and the Recirculation valve.

The EGR module depends on the pressure ratio between its inlet and outlet (p_{scav}/p_{exh}), the blower speed N_{blow} and the change over valve opening position u_{COV} as seen in Figure 3.10.

Figure 3.10: Inputs and outputs of the EGR block

3.4.1 Blower

The EGR blower performance map supplied by the manufacturer consists of different diffuser positions with a unique speed line for each position. The map is expressed in a dimensionless space, the Head

Coefficient (Ψ) and the Flow Coefficient (Φ). Both dimensionless parameters are calculated with equation 3.30, these parameters are found in (Wahlström and Eriksson 2011) and (ISO-5389 2005).

$$\Phi = \frac{Q}{N\,\pi\,R^3} \qquad\qquad \Psi = \frac{2\,c_p T\left(\Pi^{\frac{\gamma-1}{\gamma}} - 1\right)}{(N\,R)^2} \tag{3.30}$$

where N is the blower angular speed, Π is the pressure ratio over the blower, which corresponds to (p_{scav}/p_{exh}) since all pressure drops of the EGR components are neglected. And Q is the volumetric flow rate which can be calculated as the mass flow divided by the density ρ. To calculate the gas density the ideal gas law is applied resulting in $\rho = p/\left(R_s\,T\right)$.

The performance map of the EGR blower is shown in appendix A. The irregular shape of the speed lines indicates that the data points of the map corresponds to measured data. The unique speed line describing each diffuser position corresponds to $1040\,rad/s$.

The affinity laws are used to predict the blower performance when it is operated at a different speed than the one specified in the map. Since the impeller size is always constant, the following affinity laws are valid (Lewis 1996).

$$\Phi_i = \Phi_{ref} \qquad \rightarrow \qquad Q_i = \frac{N_i}{N_{ref}}\,Q_{ref} \tag{3.31}$$

$$\Psi_i = \Psi_{ref} \quad \rightarrow \quad \Pi_i = 1 + (\Pi_{ref} - 1)\left(\frac{N_i}{N_{ref}}\right)^2 \tag{3.32}$$

The subindex ref represents to the known speed line ($1040\,rad/s$) and the subindex i represents to any other blower speed.

Rearranging equation 3.30 it is possible to plot the blower map in terms of corrected mass flow versus the pressure ratio. The correction of the blower speed and the mass flow are the same as the ones defined in 3.2. Figure 3.11[3] shows the result of applying the affinity laws to both diffuser positions 2 and 4. The regions of the map outside the speed lines area needs to be extrapolated. The blower angular speed operational range found in the datasets reside between $550\,rad/s$ to $1000\,rad/s$, a speed line is plotted every $50\,rad/s$.

As mentioned before, the diffuser position is kept constant in all datasets, with a constant value of 19%. In order to know what diffuser position corresponds to a 19%, the maximum diffuser position ($Diff_{max}$) and minimum diffuser position ($Diff_{min}$) are used. Equation 3.33 shows how a diffuser percentage is related to a specific position.

$$u_{Diff_i}[\%] = \frac{Diff_i - Diff_{min}}{Diff_{max} - Diff_{min}} = \frac{Diff_i - 2}{10 - 2} \tag{3.33}$$

where the subindex i represents any diffuser position between the maximum and the minimum. The resulting position corresponding to a 19% is 3.5. Since this position is between two diffuser positions specified in the map, the speed line corresponding to 3.5 needs to be interpolated.

The interpolation of the intermediate diffuser position carried in this project is inspired in the methodology presented by (Eriksson 2007). The methodology consists of fitting a superellipse to describe the speed lines. The mathematical expression of a superellipse is shown in equation 3.34. A superellipse can be characterized by only three parameters, which are the two intersections with the axis and the exponent n.

$$\left|\frac{\Phi}{a}\right|^n + \left|\frac{\Psi}{b}\right|^n = 1 \tag{3.34}$$

[3]The axis are not visible due to confidentiality reasons

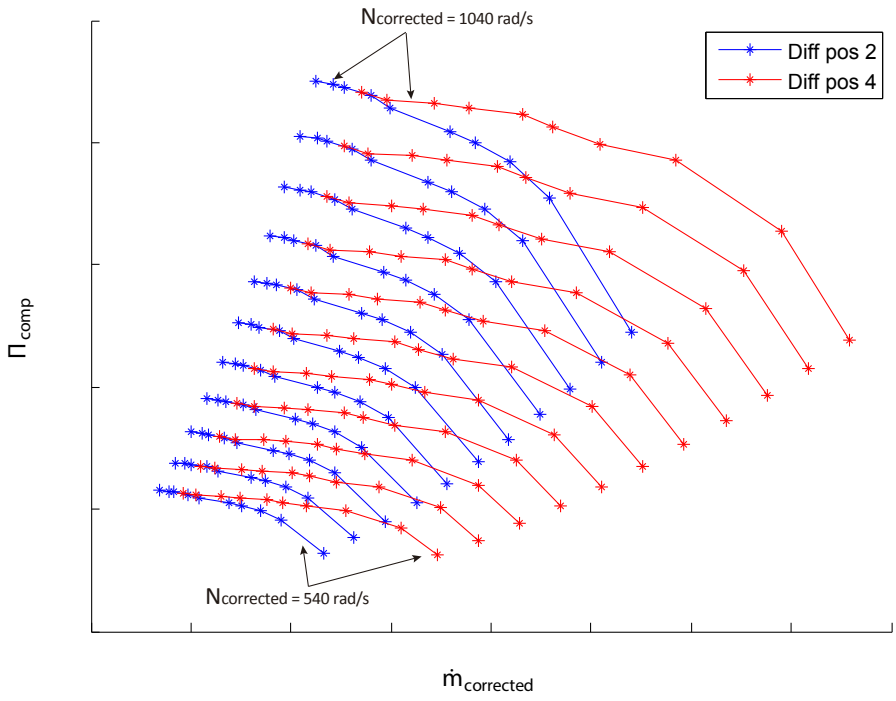

Figure 3.11: EGR Blower performance map for diffuser positions 2 and 4

where a corresponds to the intersection with the Φ axis and b to the intersection with the Ψ axis. The parameter n describes the shape of the super ellipse. For $n = 2$ a circle is obtained, and the higher n is the more it will resemble a rectangle. For further information on superellipses refer to (Weisstein n.d.).

Each of the diffuser positions speed lines is fitted with a superellipse. The three parameters describing a superellipse are estimated with a nonlinear regression, the fitted model is the ellipse equation 3.34 isolating the variable Φ. The MATLAB function ***Nonlinear.Fit*** from the Statistics Toolbox is used for this purpose since it allows the user to define the specific model to be fitted. To evaluate the goodness of the fit the Root Mean Square Error (RMSE) obtained in each regression is used, the results are shown in Table 3.1.

Diffuser position	2	4	6	8	10
Regression RMSE	0.0085	0.0123	0.0342	0.0063	0.0014

Table 3.1: Goodness of the nonlinear regressions obtained when fitting superellipses

The goodness of the fit is considered to be acceptable. The estimated coefficients for the different diffuser positions are plotted together in Figure 3.12 to analyze the tendency of the parameters with the diffuser positions.

A tendency is observed between the ellipse parameters and the diffuser positions 2, 4 and 6, but the tendency is not followed by the last two diffuser positions. The interpolation is only based on the ellipse coefficients of positions 2 and 4 since the tendency is approximately the same as if position 6 is also considered. A linear interpolation between positions 2 and 4 is carried out to estimate the parameters a, b and n for the diffuser position 3.5. Figure 3.13[4] shows fitted superellipse for diffuser positions 2 and 4 with black dashed lines, and the interpolated superellipse for the diffuser position 3.5 in green.

[4]The axis are not visible due to confidentiality reasons

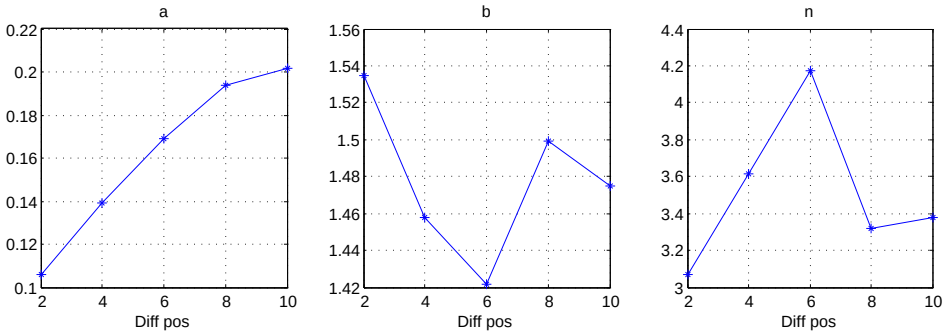

Figure 3.12: Superellipse parameters in terms of diffuser position

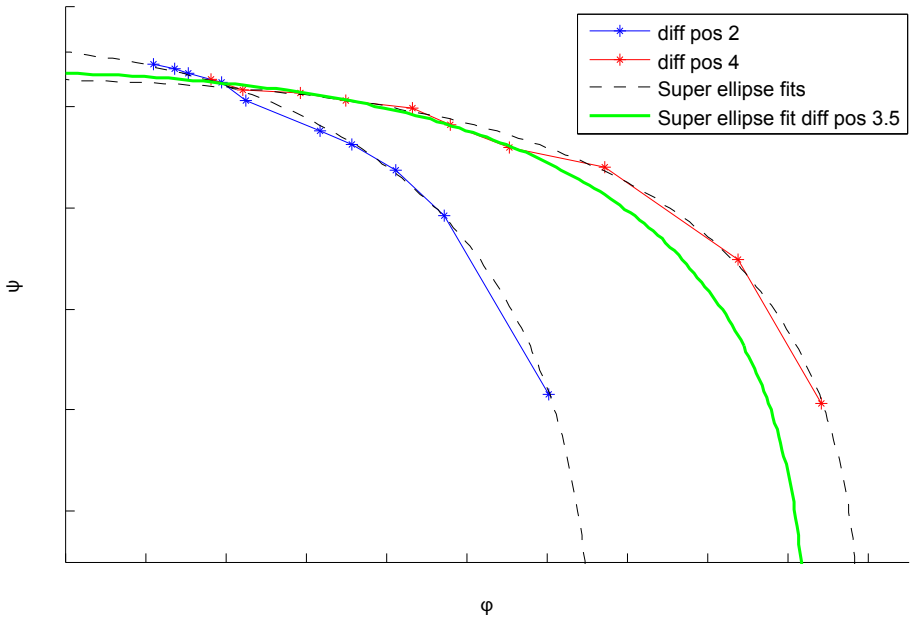

Figure 3.13: Fitted superellipse for diffuser position 2 and 4. Interpolated superellipse for diffuser position 3.5

The final coefficients describing the superellipse for the diffuser position 3.5 are shown in equation 3.35.

$$\Phi = 0.1308 \left(1 - \left(\frac{\Psi}{1.4771}\right)^{3.4785}\right)^{\frac{1}{3.4785}} \tag{3.35}$$

To summarize the EGR blower section, the solving sequence applied at each simulation step is shown in equation 3.36. The pressure ratio Π_i and the blower speed N_i correspond to the EGR blower inputs, and the subindex ref refers to the reference blower speed specified in the map $1040\ rad/s$.

$$\Pi_i \xrightarrow[N_i]{Eq[3.32]} \Pi_{ref} \xrightarrow{Eq[3.35]} Q_{ref} \xrightarrow[N_i]{Eq[3.31]} Q_i \xrightarrow{Eq[3.30]} \dot{m}_{blow} \tag{3.36}$$

3.4.2 Recirculation valve

MAN engineers informed of a leakage in the recirculation valve when the valve was closed, whose magnitude is unknown. It is important to consider the leak in the model since the leak mass flow $\dot{m}_{leak}$ should be subtracted from the estimated blower mass flow $\dot{m}_{blow}$, as shown by equation 3.37. The function $f\left(u_{COV}\right)$ represents the model of the COV and is derived in the following section.

$$\dot{m}_{egr} = \left(\dot{m}_{blow} - \dot{m}_{leak}\right)\ f\left(u_{COV}\right) \tag{3.37}$$

To model the leak the orifice approximation shown in equation 3.38 is used

$$\dot{m}_{leak} = A_{leak} \frac{p_{scav}}{\sqrt{R_{exh}\, T_{scav}}} \sqrt{\frac{2\,\gamma_{egr}}{\gamma_{egr} - 1} \left(\frac{p_{scav}}{p_{exh}}^{\frac{2}{\gamma_{egr}}} - \frac{p_{scav}}{p_{exh}}^{\frac{\gamma_{egr}+1}{\gamma_{egr}}} \right)} \tag{3.38}$$

where A_{leak} is the area of the orifice representing the leakage and γ_{egr} is the heat capacity ratio of the EGR gas. The orifice area is considered a tuning parameter to fit the measured EGR mass flow $\dot{m}_{EGR}$. These measurement is not affected by the leak since the sensor is placed prior to the cooler.

3.4.3 Change Over Valve

The COV implies a flow restriction when it is not fully opened. Figure 3.14(A) shows the EGR mass flow $\dot{m}_{egr}$ and the COV opening percentage corresponding to the EGR start up found in dataset 1. It is observed that the COV is only restricting the mass flow in the range from 0% to 45% of the COV opening (vertical dashed line). To model such behavior, an exponential decay is used to match the measured mass flow as shown in equation 3.39.

$$f\left(u_{COV}\right) = \left(1 - e^{-\frac{1}{\tau_{cov}} u_{cov}}\right) \tag{3.39}$$

The time constant of the exponential decay is tuned to match the measured mass flow in chapter 5. Figure 3.14(B) shows the $f\left(u_{COV}\right)$ results obtained when comparing three different time constants with the same u_{COV} shown in 3.14(A).

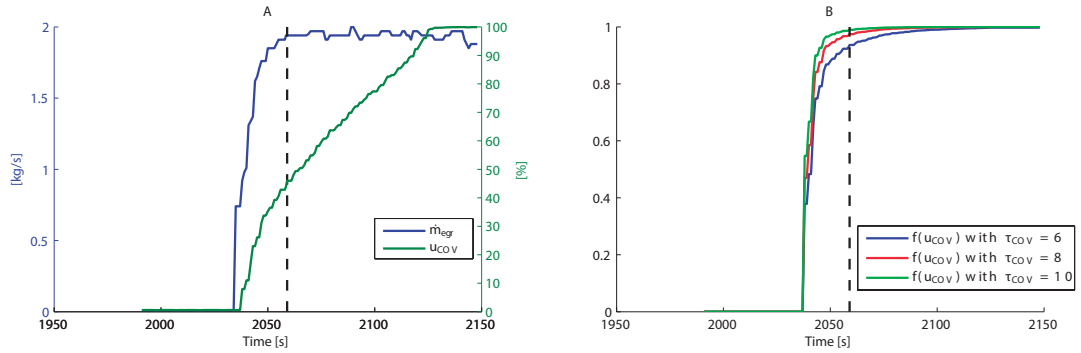

Figure 3.14: (A) COV influence to the EGR mass flow. (B) Results of the COV model using different time constants.

CHAPTER 4

Model parameters

This chapter presents the determination of the model parameters, some of them can not be determined precisely and in those cases realistic bounds are determined.

4.1 Geometrical and inertial parameters

In this section the presented parameters have been provided by MAN Diesel&Turbo .

Description	Nomenclature	Value	Units
Turbocharger moment of inertia	J_{TC}	1.893	$kg\,m^2$
Volume Scavenging manifold	V_{scav}	16.7	m^3
Volume Exhaust manifold	V_{exh}	8.7	m^3
Compression Volume	V_{comp}	0.02416	m^3
EGR Blower blade radius	R_{blow}	0.1498	m

Table 4.1: Summary of the geometrical and inertial parameters

The volumes of the scavenging and exhaust manifolds are estimations obtained by adding all the volumes of the manifold components. These estimations are subjected to which manifold components are included or neglected as part of the manifold volume, i.e. the compressor outlet and the turbine inlet housing are not included.

The volume of the EGR loop is not included in either of the manifolds volume since the EGR system is not always active. The compression volume is estimated by the PMI[1] system and it is assumed to be reliable.

4.2 Gas Mixtures

In the air path system there are up to three different gas mixtures present: the atmospheric air, the scavenge manifold gas and the exhaust manifold gas. If the EGR system is not active, then the scavenge manifold gas corresponds to atmospheric air. The composition of each manifold is defined as a mixture of atmospheric air and combustion products.

4.2.1 Mixture compositions

The atmospheric air composition used in the model is obtained from (Williams n.d.). The volumetric fractions of the species for both compositions are shown in table 4.2. All volumetric fractions are based on

[1] System pressure analyzer

a dry atmosphere, the H_2O content varies depending on the relative humidity (RH) and the atmospheric pressure. The mass fraction of water in the atmosphere is about $1\ \%$ percent, but it can be up to $4\ \%$ percent under extreme conditions as stated in (Heywood 1988). In the next section the water content in the atmosphere is investigated.

Dry atmosphere Species	N_2	O_2	CO_2	Ar
Molar fraction atmosphere [%]	78.08	20.95	0.04	0.93

Table 4.2: Dry Atmospheric composition

The combustion products composition are characterized by the stoichiometric reaction 3.11. The resulting molar fractions are shown in table 4.3. The molar weight of the combustion products mixture are also calculated with (3.13).

Combustion product species	N_2	CO_2	H_2O	Ar
Molar fraction [%]	73.18	13.36	12.55	0.87

Table 4.3: Stoichiometric combustion products composition

The exhaust and scavenge manifolds gases are mixtures of air and combustion products. The oxygen mass fractions O_{scav} and O_{exh} are used to describe the air fraction for a mixture as shown in equation 4.1. The capital X indicates that the fraction is mass based.

$$X_{air_{mix}} = \left(1 - X_{prod_{mix}}\right) = \frac{O_{mix}}{O_{amb}} \tag{4.1}$$

4.2.2 Considering Relative Humidity

Relative humidity is defined as the partial pressure of the water vapour in a mixture divided by the saturation pressure. The partial pressure is equivalent to the molar fraction assuming a mixture of ideal gases. Then the molar fraction of water of a mixture can be described with equation 4.2.

$$x_{H_2O_{mix}} = \frac{p_{H2O}}{p_{mix}} = \frac{RH}{100}\left(\frac{P_{sat}\left(T_{mix}\right)}{p_{mix}}\right) \tag{4.2}$$

where the saturation pressure can be calculated as a function of temperature as shown in equation 4.3 obtained from (IMO 2008).

$$\begin{aligned} p_{sat}\left(T_{mix}\right) = -3.115\,221 \times 10^{-8}\, T_{mix}^5 + 8.105\,25 \times 10^{-6}\, T_{mix}^4 - 7.477\,123 \times 10^{-5}\, T_{mix}^3 \\ + 0.0168891\, T_{mix}^2 + 0.2660089\, T_{mix} + 4.856884 \end{aligned} \tag{4.3}$$

where T_{mix} needs to be in $[^\circ C]$ and the resulting saturation pressure is in $[mmHg]$. To obtain the composition of a humid atmosphere, the dry atmospheric composition is scaled by multiplying each molar fraction by $(1 - x_{H_2O_{amb}})$.

The water content is calculated for the different datasets using the measured ambient relative humidity, pressure and temperature. The results obtained show a maximum content of 0.025% in all datasets. Since this percentage is considered to be insignificant, the model is simplified by assuming no water content in atmospheric air.

4.2.3 Thermodynamic parameters

The thermodynamic parameters used throughout the model are: the specific gas constants of the mixtures $R_{specific}$, the constant pressure heat capacity c_p, the constant volume heat capacity c_v and the heat capacity ratio γ. These parameters depend on the temperature and composition of a mixture.

In the two previous projects (Mahler 2013) and (Pedersen 2013) these parameters were based on temperatures commonly found in 4-stroke engines, which are higher than the temperatures commonly found in 4T50ME-X. Aiming to obtain more accurate thermodynamic parameters, these are determined based on the mean value of the measured temperatures in dataset 1: $T_{scav} = 300K$ and $T_{exh} = 650K$.

The specific gas constant R_{mix} is calculated dividing the universal gas constant by the molar weight of a mixture. The universal gas constant is $R = 8.314 \left[\frac{J}{molK}\right]$ for an ideal mixture of gases. The $c_{p_{mix}}$ of a mixture is calculated as the sum of the molar fractions of each element multiplied by the respective c_{p_i} (Heywood 1988).

$$c_{p_{mix}} = \sum_i x_i \, c_{p_i} \tag{4.4}$$

The constant pressure heat capacity c_{p_i} of an element is temperature dependent, such variation has been parameterized in many tables. In this model the NASA polynomials from the open source project CANTERA Goodwin (2013) are used. There are two different polynomials depending on the temperature, one for temperatures between $300K - 1000K$ and the other polynomial that covers the temperature range $1000K - 5000K$. Since none of the temperatures in the air path system rise higher than $1000\ K$, only the 4^{th} order polynomial covering such range is used. Equation 4.5 shows how the polynomial is used to calculated cp_i in a mass basis.

$$c_{p_i} = 1000\ R_{mix}\ \left(a_0 + a_1 T + a_2 T^2 + a_3 T^3 + a_4 T^4\right)\ \left[\frac{J}{kg\ K}\right] \tag{4.5}$$

The c_p is calculated for air and combustion products using the molar compositions from tables 4.2 and 4.3. The c_p for the scavenging and exhaust mixtures are calculated using equation 4.6

$$c_{p_{mix}} = x_{air_{mix}} c_{p_{air}} + (1 - x_{air_{mix}})\, c_{p_{prod}} \tag{4.6}$$

The c_v of the mixtures is calculated and then the heat capacity ratio γ_{mix} is also determined. Equation 4.7 shows how both parameters are defined.

$$c_{v_{mix}} = c_{p_{mix}} - R_{mix} \qquad\qquad \gamma_{mix} = \frac{c_{p_{mix}}}{c_{v_{mix}}} \tag{4.7}$$

The thermodynamic parameters obtained for the different gas mixtures are shown in table 4.4. The EGR gas represents the exhaust manifold mixture but with the scavenging temperature. The calculations have been carried out at two different situations, one with no EGR and the other one corresponding to a situation with EGR. The oxygen content in the scavenging and exhaust manifolds for the situation with out EGR are 0.2095 and 0.165 respectively, and for the EGR situation are 0.19 and 0.139 respectively. To validate the results, the software CHEPP (Eriksson 2005) is used to calculate some of the parameters.

The variations between the situation with and without EGR represent an increase smaller than 2% of the value for all the thermodynamic parameters. It is assumed that the changes in the thermodynamic properties of the gases due to recirculating exhaust gas can be neglected. The calculated parameters corresponding to the situation without EGR are the ones used in the model. A sensitivity test regarding the two sets of parameters will be carried out in chapter 6. The differences in the results obtained with the software CHEPP are also under 2% of the values and therefore these parameters are considered valid.

Parameter	Fluid	No EGR	No EGR (CHEPP)	EGR	EGR (CHEPP)
γ	Amb	1.4006	1.4006	1.4006	
	Scav	1.4006	1.4006	1.3978	
	Exh	1.3614	1.3602	1.358	1.357
	EGR	1.393		1.3906	
$R_{specific}$	Scav	287.16	287.04	287.139	
	Exh	287.1		287.083	
c_p	Amb	1003.9	1003.51	1003.9	
	Scav	1003.9	1003.51	1008.9	
	Exh	1081.4	1086.7	1093	1094
	EGR	1017.6		1022	
c_v	Scav	716.74	716.46	721.77	
	Exh	794.33	798.9	801.93	806.4

Table 4.4: Summary of the thermodynamic parameters for the gas mixtures present in the system

4.2.4 Fuel parameters

The two parameters used in the modeling chapter which depend on the fuel type are the Low Heating Value (LHV) and the molar relation between Carbon and hydrogen y. The mass fractions X_i and molar weights MW_i of both C and H are used to calculate y as shown in equation 4.8.

$$y = \frac{X_H \, MW_H}{X_C \, MW_C} \tag{4.8}$$

The fuel used at MAN Diesel&Turbo research center is Marine Gas Oil (MGO). It has been possible to examine the results from multiple Ultimate Analysis done to three different fuel batches supplied to the MAN test facility in the past years. Moreover none of the batches were used during the datasets. To be able to compare the Ultimate Analysis results with another source, in (ENTEC 2002) the same parameters are presented based on averages from 43 analyses of MGOs from ships operating in northern EU seas. Table 4.5 summarizes the fuel properties, the last column corresponds to the $A2F_s$ calculated with equation 3.12.

Fuel type	C [%]	H [%]	N [%]	LHV [MJ/kg]	$A2F_s$
Marine Gas Oil (MGO)	86.74	13.23	<0.1	42.65	14.527
Ultimate Analysis 1 - Gasoil	86.6	12.9	<0.1	42.73	14.46
Ultimate Analysis 2 - Gasoil	86.7	13.1	<0.1	42.71	14.496
Ultimate Analysis 3 - Gasoil	86.5	13.5	<0.1	42.78	14.558
Ultimate Analysis mean				**42.74**	**14.5**

Table 4.5: Fuel properties obtained from Ultimate Analysis. Calculated $A2F_s$ for each fuel.

The different LHV between the Ultimate Analysis with the values found in (ENTEC 2002) indicates a higher fuel quality used at the Research Center compared to fuel used in real vessels. The mean value of LHV and $A2F_s$ considering only the ultimate analysis is used.

4.3 Seiliger cycle parameters

In this section the parameters used while modeling the Seiliger cycle are described. First the scavenging and trapped efficiencies are discussed. Then the ECS internal parameters are used to estimate the volumes at EVO (V_4) and EVC (V_1). Finally the polytropic coefficients and the fraction of fuel burned at constant volume are calculated from in-cylinder pressure measurements.

- Scavenging efficiency η_{scav} and trapping efficiency η_{trap}

(Andersen et al. 2013) carried extensive investigation of the scavenging process of the 4T50ME-X trough CFD simulations. The results presented in (Andersen et al. 2013) correspond to situations with the auxiliary blowers running, such results can not be used as a reference since both efficiencies are increased by the blowers. One of the author supplied reasonable ranges for η_{scav} and η_{trap}, but the load dependencies are still under investigation. Both efficiencies will be considered tuning parameters as long as they are kept inside the ranges specified in table 4.6.

Parameter	Upper bound	lower bound
η_{scav}	100	90
η_{trap}	55	90

Table 4.6: Scavenging and trapping efficiency bounds

Based on the discussions with MAN engineers, the tendency of the scavenging efficiency is to decrease for lower loads, which implies that more residual gas is present in the combustion chamber at lower loads. This should be validated when more results from CFD simulations are available.

The auxiliary blowers are needed at low loads to ensure a reliable scavenging process. Based on the need of auxiliary blowers at low loads and the increasing scavenging efficiency for higher loads, it is assumed that the trapping efficiency decreases when load increases. In other words, at higher loads more scavenging gas is delivered but not trapped in the cylinder.

- Volumes at $EVC\,(V_1)$ and $EVO\,(V_4)$

The ECS internal parameters consists of lookup tables for each engine running mode. Each table describes the compression ratio and EVO crank angle at five different loads. Linear interpolation is applied for intermediate loads. The lookup tables are plotted and can be found in appendix A.

The Compression ratio is defined as the TDC pressure (p_2) divided by the EVC pressure (p_1). If EVC timing is regulated to obtain the desired set point and the compression volume (V_2) is known, then the volume corresponding to EVC can be calculated with equation 4.9.

$$V_1 = V_2 \left(\frac{p_1}{p_2}\right)^{\frac{1}{\gamma_{comp}}} \tag{4.9}$$

where V_2 corresponds to the compression volume and γ_{comp} corresponds to the polytropic compression coefficient.

The crank angle corresponding to EVO is tabulated in terms of load and engine running mode. Linear interpolation is applied between the defined points. The volume of the combustion chamber can be calculated as a function of crank angle as shown in 4.10.

$$V_{cyl} = V_2 + \pi \left(\frac{B}{2}\right)^2 \left(c + \frac{s}{2} - \frac{s}{2} cos\,(\theta) - \sqrt{c^2 - \left(\frac{s}{2}\right)^2 sin^2\theta}\right) \tag{4.10}$$

where V_2 corresponds to the compression volume, B is the cylinder bore, c is the connecting rod length, s is the stroke and θ is the crank angle.

- Polytropic coefficients γ_{comp} and γ_{exp}

In the model, the compression and the expansion are considered polytropic processes, which obey the law 3.17. The polytropic coefficients γ_{comp} and γ_{exp} can be empirically estimated from in-cylinder pressure measurements.

The PMI system registers the in-cylinder pressures of each cylinder with a resolution of 0.5 crank angle degrees. PMI measurements corresponding to five different loads are used to analyze the γ's dependency with load. The average of the four cylinder is used to minimize the effect of any unbalance between cylinders. It should be noted that the 25% load corresponds to a situation with the auxiliary blowers running and therefore the estimated coefficients are not used.

If the in-cylinder pressure of a process is plotted in terms of the cylinder volume in a logarithmic scale and a linear regression is performed, then the polytropic coefficients of the process corresponds to the slope regression, as shown in equation 4.11.

$$ln\,(p) = ct - \gamma\, ln\,(V) \tag{4.11}$$

In Figures 4.1 and 4.2 the compression and expansion processes are plotted in a logarithmic scale respectively. The variables EVO and EVC are taken into consideration when specifying the crank angles at the start of the compression and the end of the expansion. The determination of the crank angle corresponding to the end of the combustion is more subjective, and thus they are determined visually. A linear regression is calculated for each load and plotted with dashed lines. In some processes a vertical offset has been introduced to avoid overlapping between the curves, while the slope of the regression is not affected by this offset.

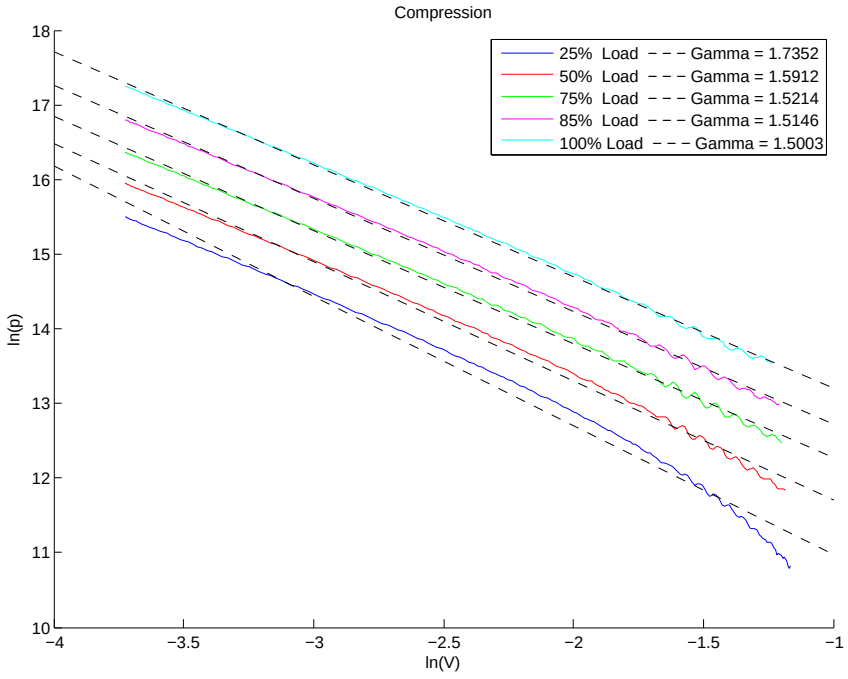

Figure 4.1: Linear regressions to estimate the compression polytropic coefficients at different loads

The results of the linear regressions are summarized in Table 4.7.

Both coefficients show a clear decreasing tendency when load increases. The γ_{comp} is always higher than 1.4 which means that the gas absorbs heat from the cylinder walls. The higher the γ_{comp} is, the more heat is absorbed by the gas. At higher loads the trapped air is more dense due to the higher pressure and

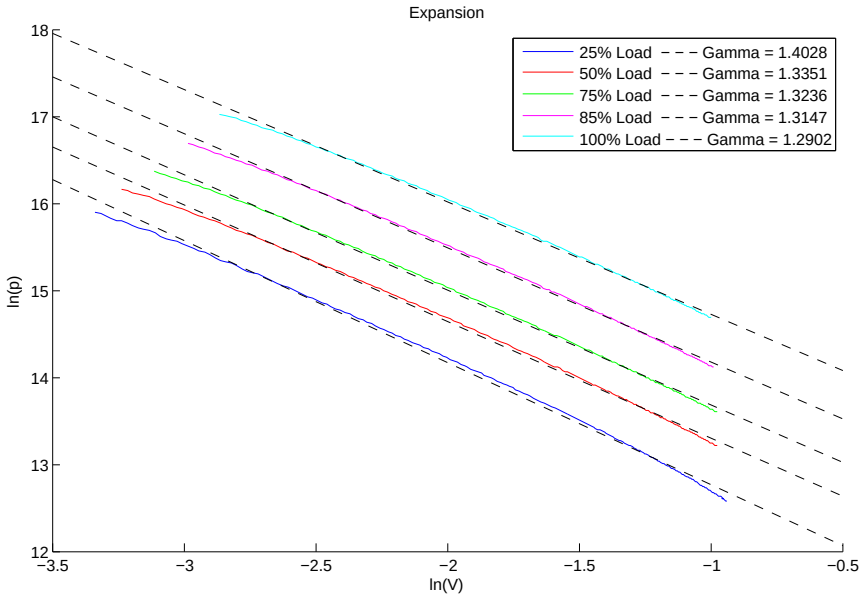

Figure 4.2: Linear regressions to estimate the expansion polytropic coefficients at different loads

	$Load[\%]$	γ_{comp}	R^2
Compression	25	1.735	98.56
	50	1.591	99.58
	75	1.521	99.83
	85	1.515	99.88
	100	1.50	99.93

	$Load[\%]$	γ_{exp}	R^2
Expansion	25	1.40	99.72
	50	1.335	99.81
	75	1.324	99.86
	85	1.315	99.87
	100	1.29	99.83

Table 4.7: Summary of the estimated γ_{comp} and γ_{exp} in terms of load

the constant temperature of the incoming gas. If two charges with different densities are compared, the temperature of the lower density charge is easier to be increased. Another fact which suggests a higher γ_{comp} for lower loads is that the cooling of the cylinder walls is proportional to load. The higher the load is, the more heat is refrigerated from the cylinder walls.

The γ_{exp} shows a decreasing tendency. This tendency is expected for higher loads because more heat is expected to dissipate to the cylinder walls as the gas temperature increases.

The goodness of the fit increases with load in both processes, witch indicates that the polytropic coefficient varies less during the processes.

In-cylinder pressure measurements at 50% load with and without EGR active are also available, although the measurements correspond to data registered six month earlier. The same procedure to estimate the γ_{comp} and γ_{exp} is carried out, and the results are summarized in Table 4.8.

	$Load[\%]$	EGR	γ_{comp}	R^2
Compression	50	Stopped	1.54	99.77
	50	Running	1.525	99.77
Expansion	50	Stopped	1.357	99.69
	50	Running	1.352	99.71

Table 4.8: Summary of the estimated γ_{comp} and γ_{exp} in terms of situations with and without EGR

The polytropic coefficients obtained with the second set of data differ from the estimated coefficient shown in Table 4.7. These differences can be explained by the different pressure sensors used in the PMI system. The interesting fact observed in Table 4.8 is the lower γ_{comp} and γ_{exp} obtained when EGR is running.

As a summary, the polytropic coefficients vary depending on load and the results shown in Table 4.7. Those are used as the initial guess in the tuning procedure. The results show a decrease of both polytropic coefficients at 50% load when EGR is active, such decrease is assumed to occur for all load levels.

- Fuel fraction burned at constant volume x_{cv}

An analytic methodology to quantify x_{cv} is explained in (Byungchan Lee and van Nieuwstadt 2013). The methodology uses the ignition delay to describe x_{cv}, and rely in the heat release curve to identify the end of the premixed combustion phase.

In this project x_{cv} is considered a constant because the heat release curve is not calculated. The magnitude of x_{cv} is unknown, and therefore, it is considered a tuning parameter.

4.4 Estimated parameters

Some of the parameters presented in the model cannot be calculated, and thus they need to be estimated from measured data. A list with the estimated parameters follows:

- A_{eng} - The cross sectional area of the engine orifice approximation.
- A_{leak} - The cross sectional area of the leak orifice approximation.
- $\tau_{O_{scav}}$ - The measurement delay of the scavenging oxygen measurement.
- τ_{COV} - The time constant for the COV model.
- $K_{O_{scav}}$ - The gain factor needed in equation 3.10.

In the next chapter, the tuning of the unknown parameters is explained.

CHAPTER 5

Model evolution and tuning

The evolution of the model is presented in this chapter. The model starts with only the turbocharger, once it is tested and verified the manifolds and the engine orifice are introduced in it. The next step is to include the estimated exhaust temperature and finally the EGR submodel is incorporated.

The tuning of the unknown parameters A_{eng}, A_{leak}, $\tau_{O_{scav}}$, τ_{COV} and $K_{O_{scav}}$ is described in the chronological order in which they are introduced in the system. The Seiliger cycle parameters calculated in the previous chapter: γ_{comp}, γ_{exh}, η_{scav}, η_{trap} and x_{cv} are also considered in the tuning procedure.

The Matlab toolbox SENSTOOLS(Knudsen n.d.) is used in (Pedersen 2013) and (Mahler 2013) to perform parameter identification using sensitivity analysis. In this project the same tool is considered, although not being able to specify the bound on which the parameters are allowed to be modified, implies that in most cases a simulation error would occur before the tuning procedure is over. Therefore this tool is not used in this project. Instead the iterative search to determine the unknown parameters is done manually. The objective sought while tuning each parameter is described.

Figure 5.1 shows the different setups tested throughout the project. The blue background measurements are used as the inputs driving the model, while the green background measurements are used to verify the different setups. The alphabetical order corresponds to the chronological evolution. Each setup is described in the following sections.

5.1 Setup A

The first component modeled is the turbocharger since the other components depend on its outputs $\dot{m}_{comp}$ and $\dot{m}_{turb}$. A GT-power model is created and coupled with a Simulink model.

Setup A consists in actuating the inlets and outlets of the turbocharger with the measured signals. p_{amb} and T_{amb} are assumed constant, and equal to the mean value of the respective measurements. Fully characterized gases at the inlet and outlet are required in the GT-Power model, for this the temperature at the compressor and turbine outlets are estimated through the definition of the compressor and turbine efficiencies. It should be noted that GT-Power does not rely on those temperatures to estimate $\dot{m}_{comp}$ and γ_{turb}. The measured turbocharger speed is used to validate the performance of the turbocharger model. Figure 5.2 shows the results obtained with this setup. The estimated turbocharger speed fits the measured data precisely.

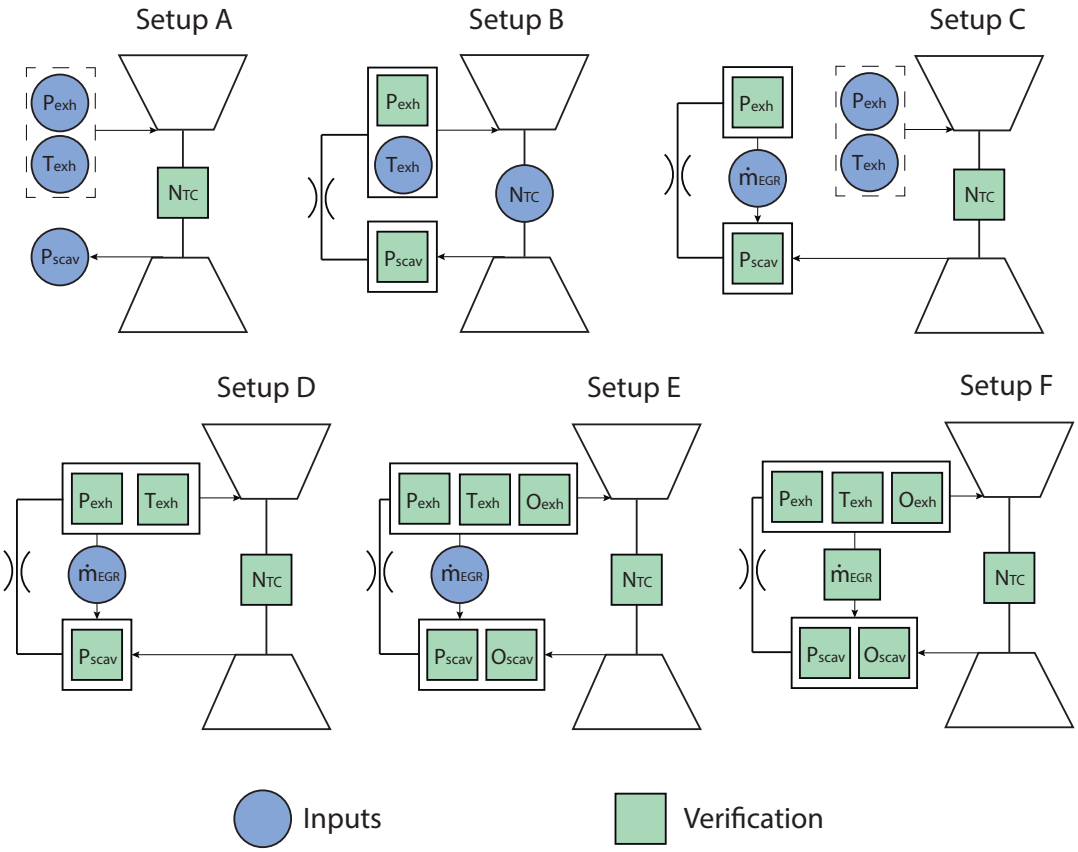

Figure 5.1: Evolution of the model

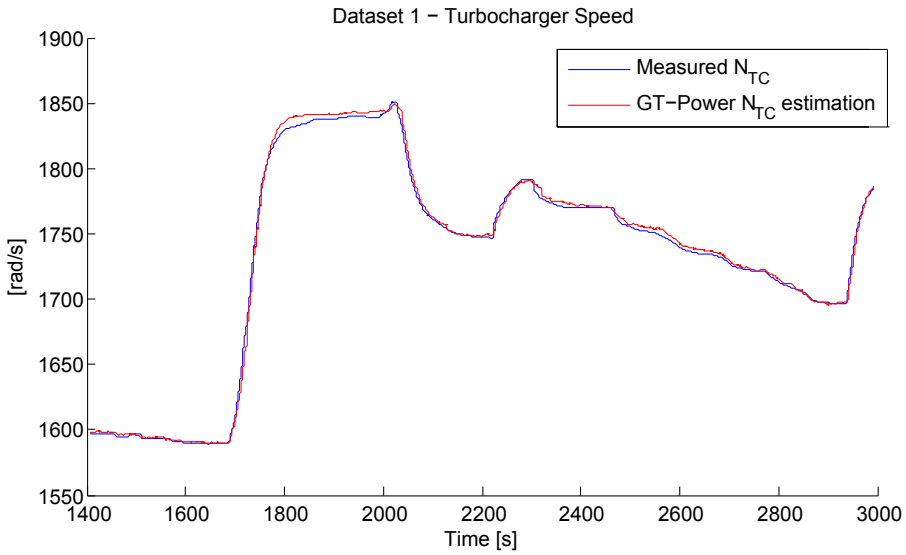

Figure 5.2: Estimated turbocharger speed using only GT-Power

5.2 Setup B

The next step is to extend the system with the engine orifice approximation and the differential equations describing the manifold pressures. The measured turbocharger speed N_{TC} is the input driving the turbine and the compressor. The measured exhaust gas temperature T_{exh} is also used as an input since its model is not derived yet. The estimated fuel mass flow is included in the model to fulfill the cylinder mass conservation. With this setup it is possible to estimate the cross sectional area of the engine orifice.

Estimated parameter:

Cross sectional area of the engine orifice A_{eng}.

Tuning objective:

The objective sought while tuning A_{eng} is to match the modeled pressure ratio over the cylinder with the measured pressure ratio. A bigger orifice area reduces the pressure ratio over the cylinder.

Result:

The resulting orifice area is $A_{eng} = 0.028[m^2]$. Figure 5.3 shows both manifold pressures and the pressure ratio over the engine. It can be observed that the tuning objective is achieved.

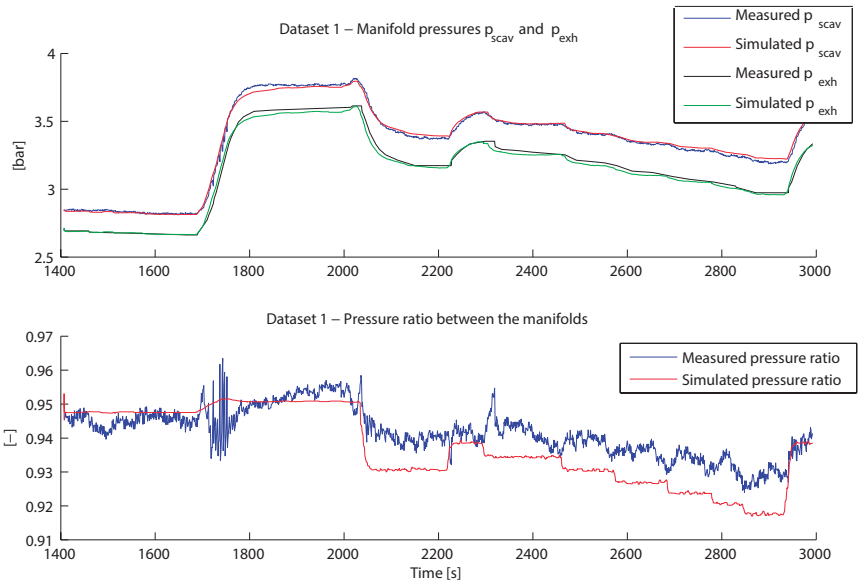

Figure 5.3: Manifold pressures and pressure ratio over the engine obtained with setup B

5.3 Setup C

The setup C consists in the characterization of the gas at the turbine inlet by the pressure p_{exh} and temperature T_{exh}. With this setup an estimation of the compressor and turbine mass flows are obtained from GT-Power.

The turbocharger speed and the pressures in the control volumes are compared to the respective measured signals. Situations with EGR active are also tested, the measured EGR mass flow is used as an input since the EGR submodel is not derived at that point.

This setup aims to validate both the GT-Power performance and the A_{eng} simultaneously. The estimated A_{eng} is capable of obtaining the correct pressure ratios at different loads.

5.4 Setup D

The next step is to derive a model for the engine outlet temperature. The Seiliger cycle presented in (Skogtjärn 2002) is modified to resemble the closed cycle of a 2-stroke engine. The early EVO and late EVC are included in the model by introducing the ECS lookup tables which define the compression ratio and the EVO crank angle in terms of load and ERM. To characterize the temperature of the charge at EVC, the scavenging and trapping efficiencies are introduced in the model.

A consequence of introducing the trapping efficiency in the model is that the exhaust manifold has two incoming flows with different temperatures. The trapping efficiency implied a reduction of the T_{exh} due to the delivered gas which is not trapped, reaching the exhaust manifold with the temperature of T_{scav}. Even though the resulting T_{exh} is reduced, the temperature obtained is too high. With the objective to reduce the estimated cycle temperature T_{cycle}, the compression and the expansion are considered polytropic processes. Using in-cylinder pressure measurements, a first estimation of their magnitude is obtained, as well as their dependency on load and ERM. All the Seiliger cycle parameters are tuned together due to the correlation between them.

Estimated parameters:

- Fuel fraction burned at constant volume X_{cv}.
- Compression and expansion polytropic coefficients γ_{comp} and γ_{exp}
- Scavenging and trapping efficiencies η_{scav} and η_{trap}

Tuning objective:

The objective sought while tuning the Seiliger cycle parameters is to minimize both manifold pressures fitting error. The GT-power model is observed to be quite sensitive to the exhaust manifold temperature.

The tuning of the Seiliger parameters is performed with the same approach the ECS regulates the compression ratio and the EVO crank angle. A lookup table defining γ_{comp}, γ_{exp}, η_{scav} and η_{trap} is tuned for the following specific loads 25%, 50%, 75%, 85% and 100%. Linear interpolation is carried to estimate the parameters values for the intermediate loads. The polytropic coefficients are also tuned for the different ERM. The fuel fraction burned at constant volume X_{cv} is considered independent from load and ERM due to the lack of knowledge about the combustion reaction. The engine running mode 2 corresponds to situations where EGR is stopped, while the mode 3 corresponds to situations where EGR is active.

When dataset 3 is tuned, an offset of 0.2 [bar] is obtained in the first 600 second. During this interval the engine is operated at 50% and 75% with EGR running, the parameters describing this operation are already tuned by datasets 1 and 2. The tuning objective for dataset 3 is to keep a constant fitting error throughout the dataset.

Result:

Dataset 1 is used to tune the parameters corresponding to the red cells in Table 5.1, blue cells are obtained with dataset 2. Finally the dataset 3 is tuned and the parameters in the green cells are obtained.

The polytropic coefficients obtained with the tuning are fairly close to the estimated coefficients shown in Table 4.7. The scavenging and trapping efficiencies are kept inside the realistic bounds stated in Table 4.6, with the exception of the scavenging efficiency at 25% load. This low efficiency is assumed to be caused by the fact that the auxiliary blowers are not active.

Load	γ_{exp}		γ_{comp}		η_{trap}	η_{scav}	x_{cv}
	ERM = 2	ERM = 3	ERM = 2	ERM = 3			
25	1.38	-	1.6	-	0.95	0.80	
50	1.335	1.323	1.565	1.56	0.90	0.91	
75	1.325	1.32	1.53	1.515	0.70	0.97	0.22
85	-	1.315	-	1.505	0.65	0.975	
100	-	1.3	-	1.5	0.60	0.98	

Table 5.1: Summary of the tuned Seiliger parameters

It should be noted that the tuning results of the Seiliger parameters depend on the dataset used in the process. Dataset 1 is used to tune the parameters at 50% and 75% load with ERM = 3, when these parameters are used in dataset 3 an offset is obtained. If the tuning order of the datasets is inverted, then the results would be different.

With the parameters from Table 4.7 a good fit of p_{scav} and p_{exh} at stable situations is obtained in all three datasets. The results are not shown since they are almost identical to the ones presented in chapter 6.

5.5 Setup E

The two differential equations describing the dynamics of the oxygen content in the manifolds are introduced at this stage. In the model, both O_{scav} and O_{exh} are mass fractions, the molar weight of the mixtures present in the manifold are needed to convert the oxygen contents from mass to molar fractions. In the case of O_{exh} it is needed to convert the measurement from wet to dry.

When the modeled O_{scav} and O_{exh} are compared with the measurements a big offset is observed. The same phenomenon was also encountered in (Mahler 2013), in that case a gain factor was introduced to compensate the offset. In this project the same the gain factor is introduced. Dataset 1 is used to estimate the magnitude of the gain factor.

Estimated parameter:

The gain factor $K_{O_{scav}}$ introduced in equation 3.10.

Tuning objective:

The objective of introducing and tuning the gain factor is to compensate the offset present in the exhaust manifold oxygen content O_{exh}.

While tuning $K_{O_{scav}}$ the estimated oxygen content can not match simultaneously the measurements at 50% load and at 75% load when EGR is active. Therefore, both situations have been penalized equally.

Result:

The obtained $K_{O_{scav}}$ is 1.09. In (Mahler 2013) the magnitude of the gain factor was 1.188. In Figure 5.4, the measured O_{exh} is shown together with the modeled O_{exh} with and without the gain factor $K_{O_{scav}}$.

A time lag between the modeled and the measured O_{scav} is observed. Therefore a measurement delay is introduced in the model in order to take the time lag into account. The magnitude of the delay is estimated comparing the modeled O_{scav} against the measured one.

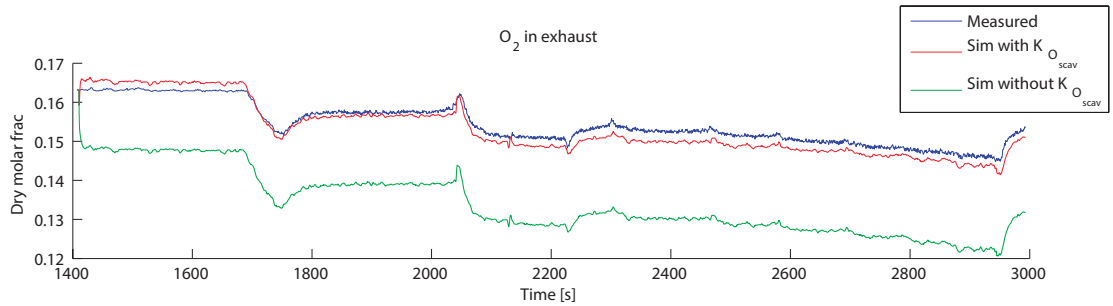

Figure 5.4: Measured and modeled O_{exh}, comparison of the results obtained with $K_{O_{scav}}$

Estimated parameter:

The O_{scav} measurement delay, $\tau_{O_{scav}}$.

Tuning objective:

The objective sought while tuning $\tau_{O_{scav}}$ is to remove the time lag between the measure and the modeled O_{scav}.

Result:

The measurement delay $\tau_{O_{scav}}$ obtained is 11.5 [s].

5.6 Setup F

Until this point the measured EGR mass flow $\dot{m}_{EGR}$ has been considered an input. The EGR blower performance map is used together with the affinity laws to describe the blower mass flow $\dot{m}_{blow}$. The known leak in the recirculation valve is modeled as an orifice. The leakage mass flow is subtracted from the estimated blower mass flow as shown in equation 3.37. The cross sectional area of the leakage orifice A_{leak} is estimated from measured data.

Estimated parameter:

Cross sectional area of the leakage orifice A_{leak}.

Tuning objective:

The objective sought while tuning A_{leak} is to quantify the leakage and consequently reduce the blower mass flow $\dot{m}_{blow}$ to match the measured EGR mass flow $\dot{m}_{EGR}$.

Result:

The tuned A_{leak} obtained is 0.0036 $[m^2]$. The results from the tuning are presented in chapter 6.

The change over valve supposes a restriction in the EGR mass flow $\dot{m}_{EGR}$. The blower mass flow that is not recirculated, is multiplied by a function $f\left(u_{COV}\right)$ which models the flow restriction created by the COV. An exponential decay is used in $f\left(u_{COV}\right)$ as shown in equation 3.39, the time constant of the exponential decay τ_{COV} defines the severity of the restriction at different u_{COV} percentages. The determination of the exponential decay time constant τ_{COV} is tuned from measured data.

Estimated parameter:

The time constant of the exponential decay τ_{COV}.

Tuning objective:

The objective sought while tuning τ_{COV} is to capture the flow restriction caused by the different opening positions of the COV. An specific event is selected to perform the tuning which is found in the time interval [2650:1930][s] from dataset 2. In this event the COV is partially closed reaching an opening position of 30% and the measured $\dot{m}_{EGR}$ shows consequent reduction of mass flow. The τ_{COV} is tuned to match the mass flow reduction.

Result:

The resulting τ_{COV} is 8. Figure 5.5 shows the measured $\dot{m}_{EGR}$, the model input u_{COV} and the modeled mass flow $\dot{m}_{EGR}$. Notice that the mass flow reduction is really accurate compared with the measured reduction.

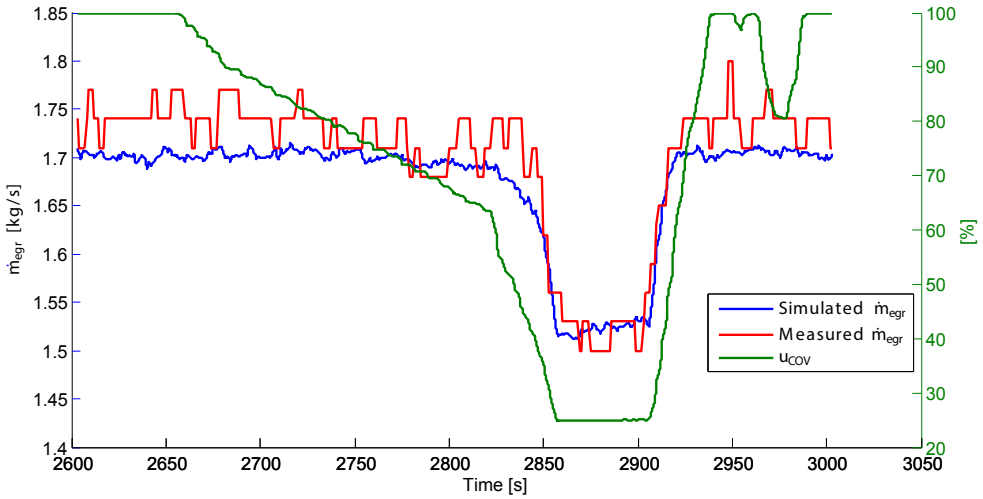

Figure 5.5: Restriction caused by the closing of the COV towards the EGR mass flow

CHAPTER 6

Model verification

In this chapter the results obtained with the model are presented and validated against measured data. First a quantitative method is described in order to evaluate the goodness of the fit. Then the results obtained in each dataset are commented. This is followed by an analysis of how sensitive is the model to parameter uncertainty. Finally the fixed step and the variable step solvers running the simulink part of the model are compared in terms of computational time.

The Normalised-Root-Mean-Square-Deviation (NRMSD) is used to evaluate the goodness of the model fit. Equation 6.1 shows how the NRMSD is defined.

$$NRMSD = 1 - \frac{\sqrt{\frac{\sum_{t=1}^{n}(y_t - \hat{y}_t)^2}{n}}}{y_{max} - y_{min}} \tag{6.1}$$

where y corresponds to measured variable, $\hat{y}$ is the estimated variable, n is the length of the dataset used, y_{max} and y_{min} are the maximum and minimum values of the variable which definethe range of the values observed throughout the dataset. A drawbacks when evaluating the model fit with the NRMSD is that it does not provide any information of the quality of the fit during transients.

6.1 Simulation results

The results presented in this section are generated with the complete model, the only input signals used are: load, COV opening percentage, EGR blower speed and engine running mode. The VGT is kept constant in all datasets. The simulation results obtained from datasets 1 and from validation dataset 4 are shown in the following sections. The remaining plots are gathered in Appendix C.

6.1.1 Manifold pressures

The estimated scavenging pressure from datasets 1 and 4 are compared to the measured pressure in Figure 6.1. For the same datasets, the exhaust manifold pressures are compared in Figure 6.2.

In dataset 1, the model follows the scavenging and the exhaust pressures accurately throughout the dataset. The correct steady state pressures are obtained at both 50% and at 75% load as well as in situations when EGR is active. It is observed in Figure 6.1 that the estimated pressures show a faster response compared to the measured pressures during the load transient. When EGR is started up at second 2050 the model response is again faster than the measured pressures.

Both estimated pressures in dataset 4 show a faster response compared to the measured pressures. A negative offset of approximately 0.1 [bar] is observed at 75% load, and an offset of approximately 0.15 [bar]

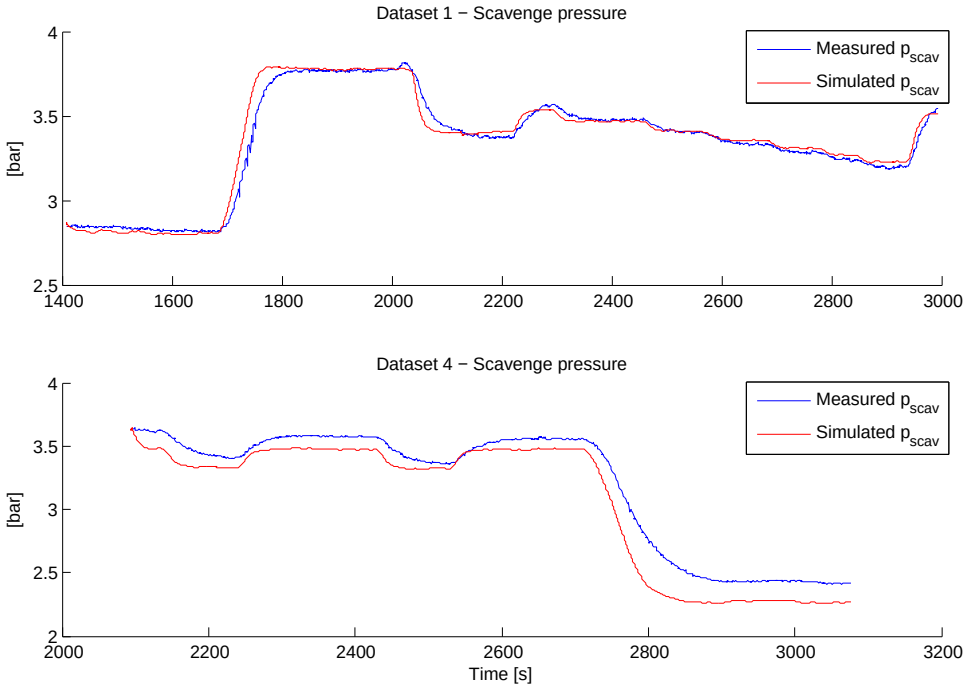

Figure 6.1: Comparison between estimated and measured scavenge manifold pressure

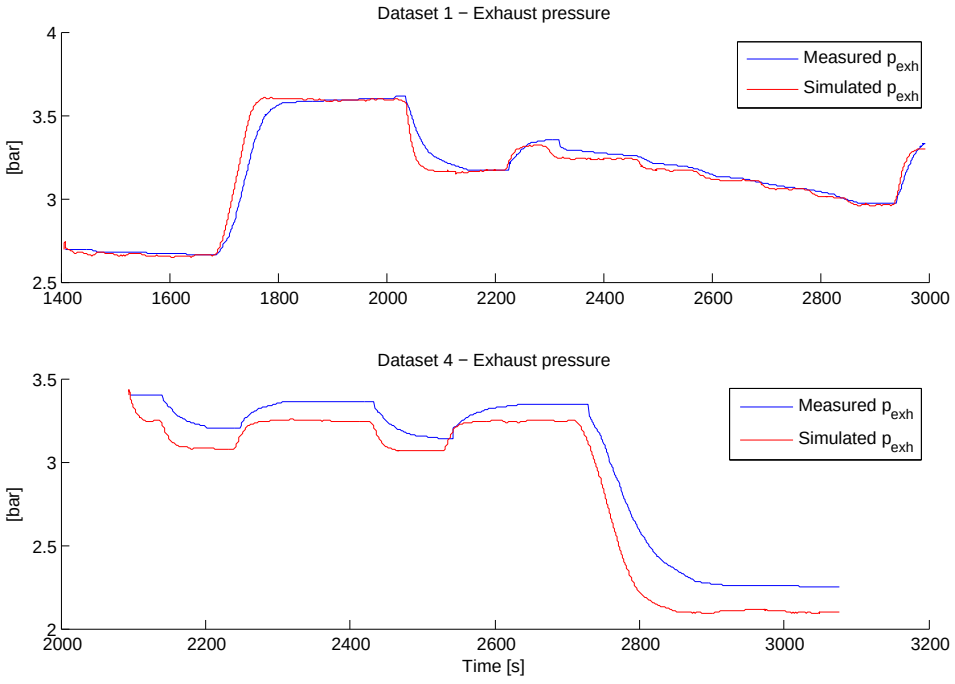

Figure 6.2: Comparison between estimated and measured exhaust manifold pressure

at 50% load. On the contrary, a positive offset of approximately 0.2 [bar] is observed in dataset 3, both datasets are is operated with the same load and the same range of EGR mass flows.

In datasets 2, 5 and 6 C the absolute pressures in steady state situations are reached with an acceptable

accuracy. The model follows correct dynamic tendencies during load steps as well as in EGR blower steps. Although the fast response during transients observed in the previous datasets is also noticed in these datasets.

6.1.2 Turbocharger speed

The estimated turbocharger speed obtained from the GT-Power is compared to the measured turbocharger speed, Figure 6.3 shows the results obtained for datasets 1 and 4.

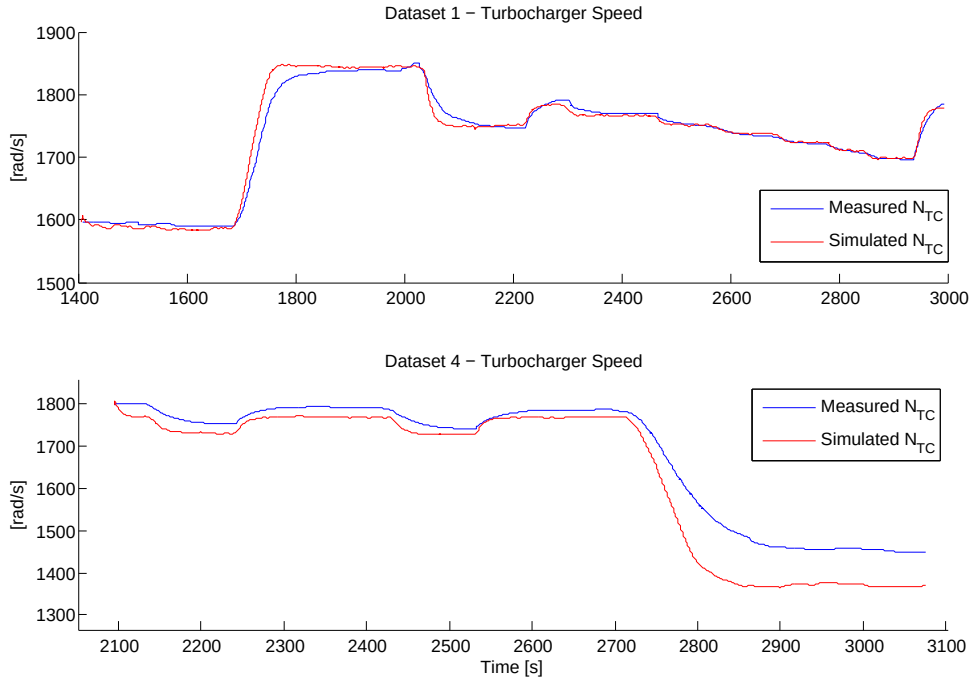

Figure 6.3: Comparison between estimated and measured turbocharger speed

It is observed a consistent tendency among the manifold pressures and the turbocharger speed in all datasets. Furthermore, the model shows a faster turbocharger speed response during transient operations which is concordant with the response observed in the manifold pressures.

The steady state speeds are reached in datasets 1, 2, 5 and 6 with minor offset. In dataset 4 an offset of approximately 20 rad/s is observed at 75% load [2100:2700][s], the offset increases up to 90 rad/s when load is decreased to 50% [2850:3100][s]. The offsets observed in p_{scav} and p_{exh} in datasets 4 is thought to be caused by the error fit in turbocharger speed.

An interesting feature of the GT-Power software is the possibility to analyze in which areas of the performance maps the compressor and the turbine are operated. Both the mass flow and the efficiency traces of a simulation are generated by GT-Power. All four maps are gathered in appendix A[1], they all correspond to a simulation of dataset 1. From the compressor mass flow trace it is observed that during all the simulation the compressor is operated inside the area surrounded by a dashed line, which corresponds to the area defined in the SAE performance map. The efficiency trace shows that the compressor efficiency is always higher than 82.5%. On the other hand, the figures corresponding to the turbine also show that it is operated inside the area defined in the performance map within an efficiency from 57% to 71%.

[1] Due to confidentiality reasons the appendix will not be part of the public report

GT-Power is capable of extrapolating the performance outside the area described by the SAE performance map. But no extrapolation is needed in any of the datasets for the turbine and the compressor since they are always operated inside the areas defined by the SAE maps.

6.1.3 Exhaust manifold temperature

The estimated temperature in the exhaust manifold is compared to the measured temperature. The results obtained for datasets 1 and 4 are shown in Figure 6.4.

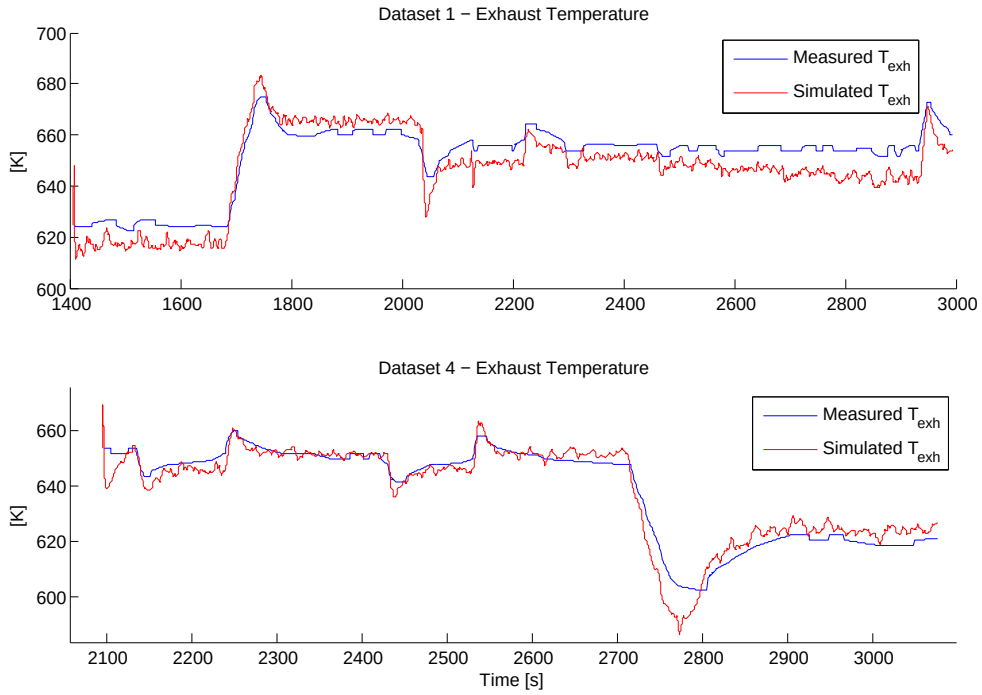

Figure 6.4: Comparison between estimated and measured exhaust manifold temperature

A negative offset of approximately -7^oC degrees is observed in dataset 1 for the exhaust manifold running at 50% load. While at 75% the offset is positive with an approximate magnitude of 6 ^oC. During the sequence of EGR blower steps, a growing offset is observed, at instant 2400[s] the offset magnitude is -5 ^oC and at instant 2860[s] the offset is approximately -13 ^oC. It is believed that the growing fitting error of the exhaust temperature affects the turbocharger module and consequently the manifold pressures. This growing offset when the EGR mass flow is increased indicates that a dependency between the EGR mass flow and the resulting Seiliger cycle temperature exists. It is believed that the scavenging and trapping efficiencies are not affected by the EGR mass flow and its been proven that the polytropic coefficients vary when EGR is activated. But not enough in-cylinder pressure measurements with different EGR mass flows is available in order to quantify the dependency between the polytropic coefficients and the magnitude of the EGR mass flow.

In datasets 3, 4, 5 and 6 the steady state temperatures are reached with small offsets. Dataset 2 is the only dataset with loads under 50%, the estimated temperature is 40 ^oC lower than the measured temperature. This is the result of tuning the Seiliger cycle with the objective to obtain a good fit of the manifold pressures. No explanation has been found which could indicate the source of this inconsistency.

The dynamic response of the estimated temperature during transients is slightly faster than the measured temperature in all datasets. Whenever a fast transient occurs, an overshoot is observed in the estimated temperature, it is assumed that there are low-pass sensor dynamics in the temperature sensor, which could be hiding the overshoot.

6.1.4 EGR mass flow

The estimated EGR mass flow is compared to the measured mass flow. The results obtained with datasets 1 and 4 are shown in Figure 6.5. The leakage mass flow is also plotted since it will be discussed.

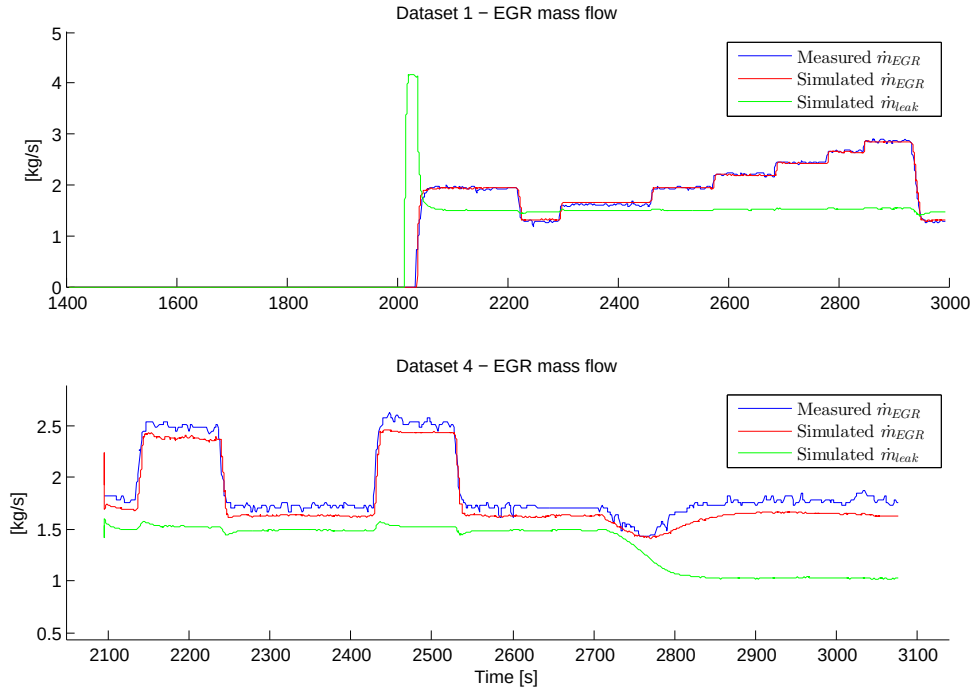

Figure 6.5: Comparison between estimated and measured EGR mass flow

The EGR mass flow fits the measured mass flow with high accuracy. In datasets 1 a sequences of blower speed steps with a magnitude of 50 rad/s is precisely captured. In dataset 4 a small offset of approximately 0.1 kg/s is observed, this offset is believed to be caused by the offset in the manifold pressures.

Dataset 3 is specially interesting since it is the only dataset where the variations of EGR mass flow are caused exclusively by load changes, the EGR blower speed is kept constant during all the dataset. The EGR model is capable of acquiring the steady state magnitudes as well as the dynamic transients of the EGR mass flow as shown in Figure C.5.

The areas in the corrected EGR blower performance map where the blower is operated are shown in Figure 6.6. The black lines are to the estimated speed lines of the diffuser position 3.5. To improve the visibility of the plot a color map is used to indicated how frequent the blower remains in each area. Notice that the X axis is expressed as corrected mass flow, this correction is explained in equation 3.2.

The use of the corrected mass flow is because the correlation between the the Flow Coefficient (Φ) and the mass flow is pressure dependent as it is observed in equation 3.30 (the density is determined from the pressure in the compressor inlet p_{exh}). Thus, from this correction in the mass flow the dependency is

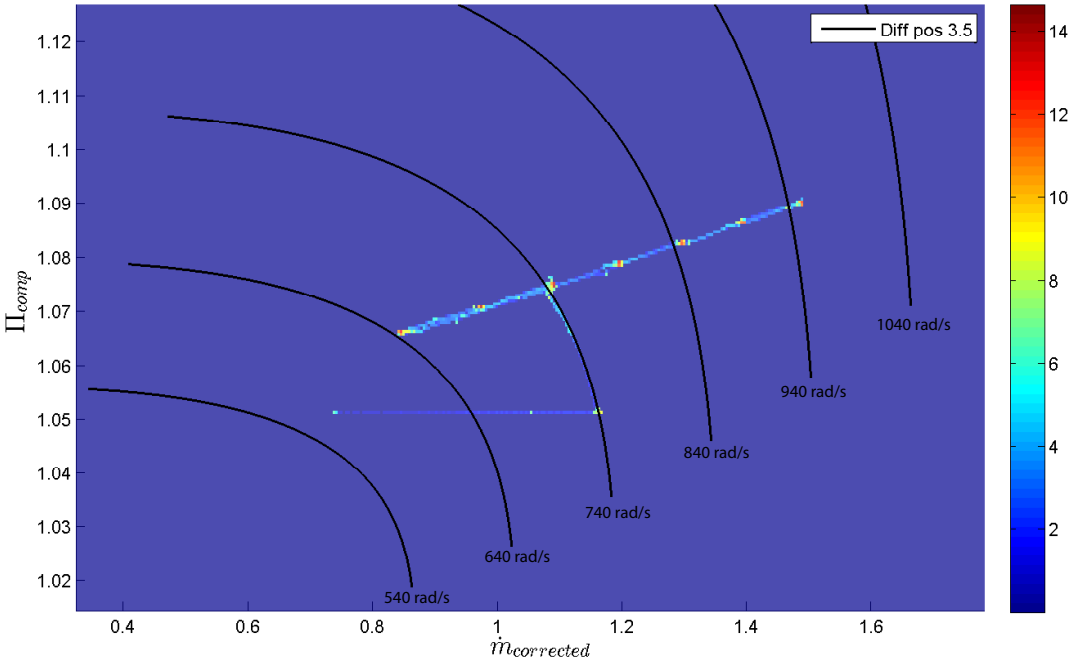

Figure 6.6: Most frequent regions where the EGR blower was operated

removed. It is also noticed that each of the blower speed steps can be seen in the color map, the red area corresponds to the stable blower speeds.

The estimated leakage flow $\dot{m}_{leak}$ has almost the same magnitude as the EGR blower flow $\dot{m}_{EGR}$. The expected $\dot{m}_{leak}$ by MAN engineers is approximately 20% of $\dot{m}_{EGR}$. The extremely high leakage flow estimated could be explained by unmodeled dynamics affecting the blower, or a flaw in the implementation of the affinity laws. Even though the magnitude of the leak is unrealistic, the overall $\dot{m}_{EGR}$ fit the measured data very accurately.

6.1.5 Oxygen content

The estimated scavenge manifold oxygen content obtained when simulating datasets 1 and 4 is compared to the measured oxygen contents in Figure 6.7. The comparison between the estimated and measured oxygen content in the exhaust manifold is shown in Figure 6.8.

In dataset 1 a visible offset can be seen in the O_{scav} when EGR is running with a magnitude of 0.0025. This offset is caused by a too low O_{exh} estimation when EGR is active. But a too high O_{exh} is estimated at 50% load when EGR is stopped. The dynamic responds of the both oxygen contents is faster than the measurements when the EGR blower speed changes, although the response when load transients occur shows the same response speed.

In dataset 4 a constant negative offset is observed in both oxygen concentrations during all the dataset. At interval [1700:2800][s] a bump is observed in the estimated O_{scav} which is not present in the measured O_{scav}. This phenomenon is believed to be caused by the lower oxygen content in both manifolds for the following reasons: the magnitude of O_{exh} is approximately 0.15 in the instant before the bump occurs, during the load transition it reaches a molar fraction of 0.165 which corresponds to situations with no EGR. If the offset was not present the increment would be smaller since the maximum oxygen content would still

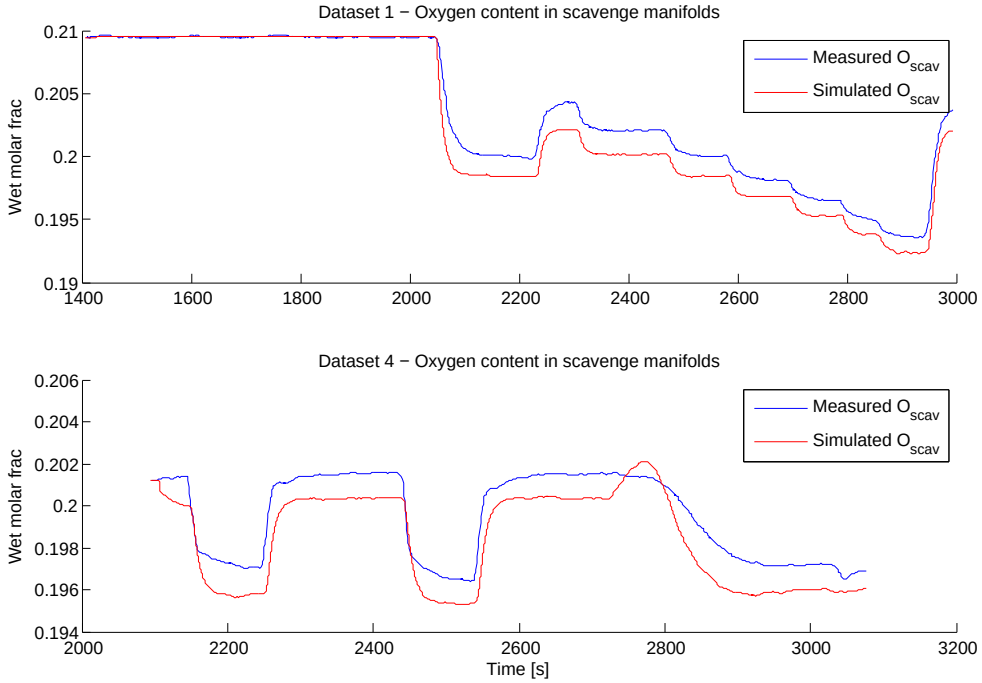

Figure 6.7: Comparison between estimated and measured oxygen content in the scavenge manifold

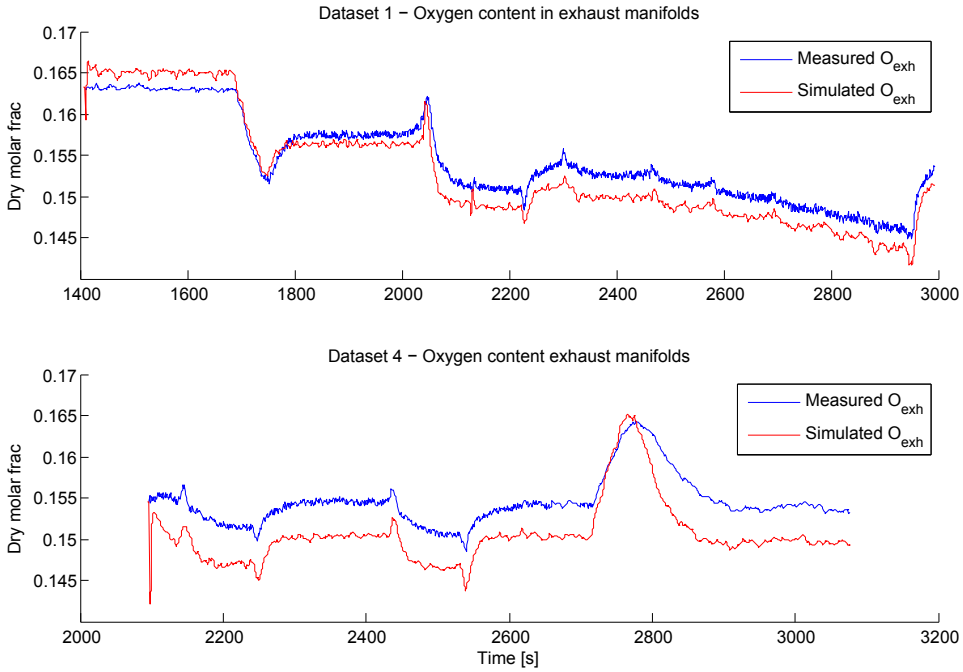

Figure 6.8: Comparison between estimated and measured oxygen content in the exhaust manifold

be 0.165. Furthermore, the lower O_{scav} estimated is more prompt to be effected by an increase of O_{exh}. Notice that the difference between measured and estimated O_{exh} corresponds to approximately 0.005, and the height of the bump is approximately 0.002.

The estimated measurement delay $\tau_{O_{scav}}$ removes the time lag between the model and the measurements

in all datasets with the exception of dataset 3. A visible time lag in O_{scav} is still present in this dataset as seen in Figure C.6. Since in this dataset the EGR mass flow variations are exclusively caused by load change, it is believed that a process delay could be the reason of the observed time lag.

The gain factor $K_{O_{scav}}$ tuned to obtain a good fit in the exhaust manifold oxygen content is needed in all dataset.

6.1.6 Results summary

The NRMSD of each variable is calculated in order to give an overview of the goodness of the complete model fit. Table 6.1 shows a summary of the results obtained while simulating each dataset.

Dataset	p_{scav}	p_{exh}	T_{exh}	N_{TC}	$\dot{m}_{egr}$	O_{scav}	O_{exh}
1	95	94	85.9	95.5	98.3	91.7	88.3
2	96.3	95.5	71.7	97.1	98.3	93.2	93
3	91.1	92.2	91.5	92.4	94.9	80.7	75.1
4	87.5	85.8	92.1	83	90.7	76	73.7
5	89.7	93.1	59.4	92.9	91.8	91.3	89.5
6	95.7	93.4	76.2	88.7	97.7	93.9	93.3

Table 6.1: Summary of all states NRMSD [%] obtained while simulating each dataset

The goodness of the fit obtained in datasets 1, 2, 5 and 6 is considered to validate the overall model, most of the variables fit the measurements with NRMSD higher than 90%. It is observed that a good fit in T_{exh} does not result in a better global fit.

It should be noted that the reason of the 59.4% obtained in dataset 5 for T_{exh} is that the estimated temperature has an offset of approximately 7 ^oC and the range of observed values ($y_{max} - y_{min}$) is approximately 20 ^oC.

To conclude, the results presented in Table 6.1 shown an acceptable fit between the model presented here and the experimental measured data.

6.2 Sensitivity analysis

In this section the sensitivity of the model versus parameter uncertainty is investigated. Dataset 1 is used to quantify how sensitive the model is to parameter uncertainty.

The parameters are modified in order to see how much the NRMSD is changed for the different variables. Table 6.2 summarizes the difference in NRMSD obtained with each parameter deviation tested, a negative values indicate a worst model fit.

A common deviation of 10% of the parameter value is selected. The scavenging temperature deviation is 5^oC, which is based on the different scavenging temperatures observed in all assessed data. The polytropic coefficients γ_{comp} and γ_{exp} are not allowed to deviated 10% because simulation errors would arise. The η_{scav} is reduced 10% because an increment would result in efficiencies higher than 100% which are not rational.

The first parameter, referred as "thermodynamic properties" are all the parameters calculated in section 4.2.3, the deviation referred as "EGR" corresponds to the parameters calculated for a situation with EGR active.

Parameter	Deviation	p_{scav}	p_{exh}	T_{exh}	N_{TC}	$\dot{m}_{egr}$	O_{scav}	O_{exh}
Thermodynamic properties	EGR	-0.5	-1.1	-2.4	-0.9	-0.1	-0.7	-3.8
T_{scav}	+5^oC	-2.3	-0.9	2.9	-2	0	0.8	1.7
γ_{comp}	+ 0.01	-0.4	-1.1	-2.3	-0.7	-0.1	-0.5	-2.62
γ_{exp}	+ 0.01	-5	-5.8	-7.7	-6	-0.6	-1.5	-8.6
η_{trap}	* 1.1	-2.7	-1.4	2.6	-2.5	-0.3	0.7	1.7
η_{scav}	* 0.9	-7.8	-5.8	2.6	-7.4	-1	1.5	2.4
x_{cv}	* 1.1	0.1	-0.1	-0.3	0	0	0	-0.5
A_{eng}	* 1.1	-0.8	-0.9	-8.3	-1	-4.9	-4.4	-0.7
A_{leak}	* 1.1	-0.4	+0.3	+0.8	-0.2	-1.3	2.7	1.5

Table 6.2: Model sensitivity due to parameters uncertainty

The model seems not to be specially effected when using the thermodynamic parameters corresponding to a situation with EGR active. The effects obtained when the fuel fraction burned at constant volume x_{cv} and the cross sectional area of the leak A_{leak} are deviated can be considered insignificant. Minor effects are obtained when deviations are introduced to: the compression polytropic coefficient γ_{comp}, the scavenging temperature T_{scav} and the trapping efficiency η_{trap}. A deviated cross sectional area of engine orifice A_{eng} only affects: the EGR mass flow, the exhaust temperature and the scavenge oxygen content, all other variables are not affected significantly.

It can be concluded that the model is significantly sensitive towards the polytropic expansion coefficient γ_{exp} and the scavenging efficiency η_{scav}.

It should be noted that from the results of the sensitivity analysis shown in Table 6.2 it seems that the tuning of $K_{O_{scav}}$ could be improved, but this is only because in dataset 1 the duration of the negative offset in O_{scav} obtained with EGR active is longer than the positive offset obtained at 50% load with EGR stopped.

6.3 Simulation times

The GT-Power solver recommended by MAN engineers is a fix step solver using Runge Kutta as its integration method, with a step size of 10 [ms].The Simulink part of the model is simulated with a variable step solver (ODE45) and with a fixed step solver (Runge Kutta) to compare the computational time. The relative tolerance in the variable step solver is set to the default value $1e^{-3}$.

Dataset	Dataset duration	Variable step (ODE45)	10 [ms] fixed step size (Runge Kutta)
1	1584 [s]	1005[s]	959 [s]
3	3806 [s]	2537[s]	2343 [s]

Table 6.3: Comparison of simulation time for different Simulink solvers

The simulation time obtained with the fixed step solver is smaller than with the variable step. The variable step solver varies the step size in order to fulfill the relative tolerance, but if the GT-Power block runs at a fixed step, then the maximum step size is limited by this block.

Based on the former results, it is recommended to use the fixed step solver since the simulation results do not differ. No further investigation in the solvers is performed.

CHAPTER 7

Conclusions and Further Work

7.1 Conclusions

In this thesis a Mean Value Engine Model of the air-path system with EGR technology for a large 2-stroke diesel engine is presented and validated.

The turbocharger model is implemented using the high fidelity simulator called GT-power. The results obtained with GT-power are accurate, which allowed the modeling of the remaining components with truthful compressor and turbine mass flows.

A modified Seiliger cycle approximation capable of taking the variable EVO and EVC into account is presented in this thesis. The engine control system lookup tables defining the set point of the compression ratio and the EVO crank angle are included in the model. Inspired in this approach the tuning of the Seiliger cycle parameters is also based on lookup tables depending on load and the engine running mode.

The model is capable of estimating the manifold pressures with a maximum estimation error of 0.2 $[bar]$ in all datasets. The oxygen contents in both manifolds are estimated with acceptable accuracy.

The fitting results obtained with the EGR module are the highest in the system. The EGR mass flow is accurately estimated in both steady states and transients. However the magnitude of the recirculated flow is not reasonable, which could indicate unmodeled dynamics or a flaw in the implementation of the affinity laws.

The sensitivity of the model against parameter uncertainty has been addressed. The sensitivity analysis shows that the model is most sensitive to the expansion polytropic coefficients γ_{exh} and to the scavenging efficiency η_{scav}.

It is concluded that the model is capable of capturing the steady state values of all the variables in the system with acceptable accuracy. The dynamic response of the model in transient operations is considered acceptable, although a generalized faster response compared to the measurements is obtained in all datasets.

It is believed that the final model presented in this thesis is a reliable dynamic engine model of the 4T50ME-X. This engine model can be used to analyze and validate the performance of new EGR controller strategies. For this reason the purpose of the thesis is fulfilled.

7.2 Further work

Over the course of this thesis, there have been observed some aspects which are worth investigating further. The most relevant improvements that could be sought in future projects are:

- A model of the turbocharger should be derived in order to remove the dependency with GT-Power. This task is thought to be easier with the presented model, because the GT-Power model can be used

as a reference for the validation process.

- The incorporation of a process delay should be investigated for situations where the variations of the EGR mass flow are the result of load changes.
- In-cylinder pressure measurements in situations with different EGR mass flows should be gathered with the purpose to study the dependency between the EGR mass flow and the Seiliger cycle.
- Further investigation should be addressed towards determining the cause of the offset detected in the exhaust manifold oxygen content.
- Heat transmission effects in the manifolds should be considered with the objective to improve the model response during transients.

CHAPTER 8

Nomenclature

Symbol	Meaning
A	Area
c_p	Heat capacity at constant pressure
c_v	Heat capacity at constant volume
D	Diameter
H	Enthalpy
J	Moment of inertia
m	Mass
$\dot{m}$	mass flow
MW	Molar weight
O	Oxygen mass fraction
p	Pressure
Q	Volumetric flow rate
R	Universal gas constant
R_i	Specific gas constant of i
RH	Relative humidity
T	Temperature
u	Input signal
V	Volume
x_i	Molar fraction of i
X_i	Mass fraction of i
γ	Heat capacity ratio
η	Efficiency
θ	Crank angle
Π	Pressure ratio
Φ	Flow Coefficient
Ψ	Head Coefficient
ω	Rotational speed

Sub-index	Meaning
amb	Ambient
$blow$	Blower
$comp$	Compression
del	Delivered
$diff$	Diffuser position
egr	EGR loop
eng	engine
exh	Exhaust
exp	Expansion
in	Inlet
out	Outlet
$prod$	Combustion products
$scav$	Scavenging
TC	Turbocharger
$trap$	Trapped
$wall$	Exhaust receiver wall

abbreviations	Description
$A2F_s$	Stoichiometric Air to Fuel ratio
AC	Air Cooler
BDC	Bottom Dead Center
CBV	Cylinder Bypass Valve
COV	Change Over Valve
ECS	Engine Control System
EDS	Engine Diagnostics System
EGB	Exhaust Gas Bypass
EGR	Exhaust Gas Recirculation
ERM	Engine Running Mode
EVC	Exhaust Valve Closing
EVO	Exhaust Valve Opening
IMO	International Marine Organization
IPC	Intake Port Closing
IPO	Intake Port Opening
LHV	Low Heating Value
MCR	Maximum Continuous Rating
MGO	Marine Gas Oil
$MVEM$	Mean Value Engine Model
$NRMSD$	Normalized Root Mean Square Deviation
SDV	Shut Down Valve
TC	Turbocharger
TDC	Top Dead Center
VGT	Variable Geometry Turbocharger
WMC	Water Mist Catcher

Bibliography

Andersen, F., Hult, J., Nogenmyr, K.-J. and Mayer, S.: 2013, Numerical investigation of the scavenging process in marine two-stroke diesel engines, *SAE/KSAE 2013 International Powertrains, Fuels & Lubricants Meeting* .

Byungchan Lee, Dohoy Jung, Y.-W. K. and van Nieuwstadt, M.: 2013, Thermodynamics-based mean value model for diesel combustion, *Eng. Gas Turbines Power 135(9), 091504 (Jul 31, 2013) (9 pages)* .

ENTEC: 2002, Quantification of emissions from ships associated with ship movements between ports in the european community, *Technical report*, European Commission.

Eriksson, L.: 2005, CHEPP – A Chemical Equilibrium Program Package for Matlab, *SAE Transactions, Journal of Fuels and Lubricants, 2004-01-1460* **4**(113), 730–741.

Eriksson, L.: 2007, Modeling and control of turbocharged si and di engines, *Oil & Gas Science and Technology - Rev. IFP 62 (4), 523 - 538* .

Gamma-Technologies: n.d., Gt suite - the leading cae platform in the engine and vehicle industry.
URL: *http://www.gtisoft.com/*

Goodwin, D.: 2013, Cantera: An object-oriented software toolkit for chemical kinetics, thermodynamics, and transport processes.
URL: *https://code.google.com/p/cantera/*

Guzzella, L. and Onder, C. H.: 2010, *Introduction to Modeling and Control of Internal Combustion Engine Systems*, Springer.

Hansen, J. M., Zander, C.-G., Pedersen, N., Blanke, M. and Vejlgaard-Laursen, M.: 2013, Modelling for control of exhaust gas recirculation on large diesel engines, *Proceedings of the 9th IFAC conference on Control Applications in Marine Systems* .

Heywood, J. B.: 1988, *Internal Combustion Engine Fundamentals*, McGraw-Hill.

IMO: 2008, Amendments to the technical code on control of emission of nitrogen oxides from marine diesel engines, *Technical report*, International Maritime Organization.

IMO: 2011, International shipping facts and figures – information resources on trade, safety, security, environment, *Technical report*, International Maritime Organization.

ISO-5389: 2005, Turbocompressors - performance test code.

Knudsen, M.: n.d., Senstools.
URL: *http://www.control.auc.dk/ mk/ExpMod/SENSTOOLS/*

Lamas, M. I. and Rodríguez, C. G.: 2012, Emissions from marine engines and nox reduction methods, *Journal of Maritime Research* **9**(1), 77–82.

Lewis, R. I.: 1996, *Turbomachinery performance analysis*, Arnold.

Mahler, J.: 2013, *Exhaust gas recirculation control for diesel engine*, Master thesis, Technical University of Denmark.

Math-Works: n.d., Simulink - the industry standard for modeling control systems.
URL: *http://www.mathworks.se/products/simulink/*

Noppenau, M. H. G.: 2012, *Dynamic performance modelling of a marine selective catalytic reactor system*, Master thesis, Technical University of Denmark.

Pedersen, N.: 2013, *Modelling and identification of exhaust gas recirculation for two stroke diesel engines*, Master thesis, Technical University of Denmark.

Rajput, R.: 2005, *Internal Combustion Engines*, Laxmi Publications.

SAE-J1826: 1995, Turbocharger gas stand test code.

SAE-J922: 2011, Turbocharger nomenclature and terminology.

Skogtjärn, P.: 2002, *Modelling of the exhaust gas temperature for diesel engines*, Master's thesis, Linköpings Universitet, SE-581 83 Linköping.

Sorenson, S. C.: 2008, *Engine Principles and Vehicles*, Technical University of Denmark. Department of Mechanical Engineering.

Tao, S.: 2012, *Control of a man diesel engine with egr*, Master thesis, Technical University of Denmark.

Theotokatos, G.: 2010, On the cycle mean value modelling of a large two-stroke marine diesel engine, *Proceedings of the Institution of Mechanical Engineers, Part M: Journal of engineering for the maritime environment* **2**24(3), 193–206.

UNCTAD: 2013, Recent developments and trends in international maritime transport affecting trade of developing countries, *Technical report*, United Nations.

Vigild, C. W.: 2001, *Internal combustion engines - Modelling, estimation and control issues*, PhD thesis, Technical University of Denmark.

Wahlström, J. and Eriksson, L.: 2011, Modelling diesel engines with a variable-geometry turbocharger and exhaust gas recirculation by optimization of model parameters for capturing non-linear system dynamics, *Proceedings of the Institution of Mechanical Engineers, Part D: Journal of Automobile Engineering July 2011 225: 960-986* .

Watson, N. and Janota, M.: 1982, *Turbocharging the Internal Combustion Engine*, Macmillan.

Weisstein, E. W.: n.d., Superellipse From MathWorld—A Wolfram Web Resource. Last visited on 21/4/2014.
URL: *http://mathworld.wolfram.com/Superellipse.html*

Williams, D. R.: n.d., Nasa - earth fact sheet. Last visited on 10/4/2014.
URL: *http://nssdc.gsfc.nasa.gov/planetary/factsheet/earthfact.html*

Appendices

APPENDIX **A**

Confidential information

This appendix is not part of the public thesis due to the non disclosure agreement between MAN Diesel&Trubo and Denmark Technical University (DTU).

APPENDIX **B**

Validation Dataset

The validation datasets are gathered in this appendix. A description of the experimental tests found in the dataset is given.

In dataset 4 two small steps of 150 $[rad/s]$ in the EGR blower speed are performed at 75% load. Then the load is reduced to 50% while the blower speed is increased.

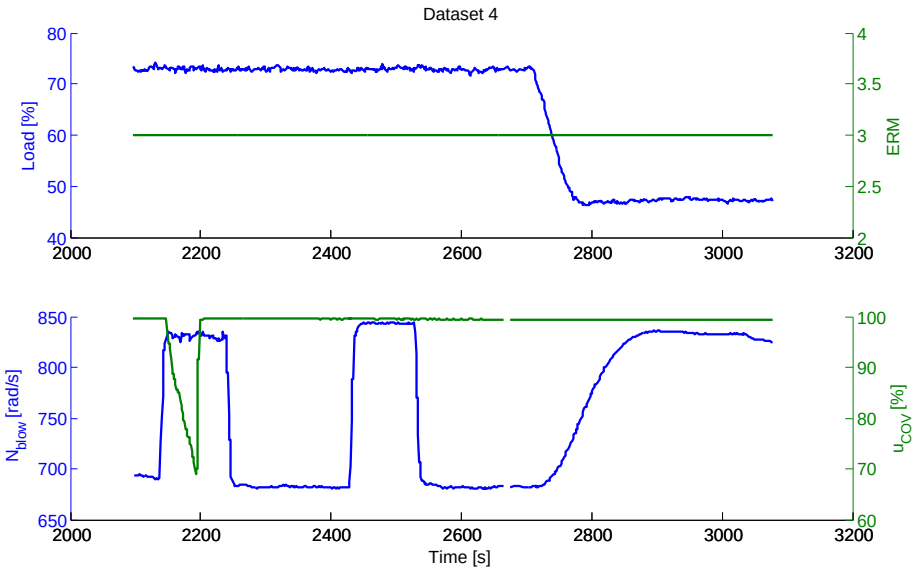

Figure B.1: Input signals from dataset 4

During all dataset 5, the load is kept constant at 50%. A sequence of 5 small steps in the EGR blower are performed.

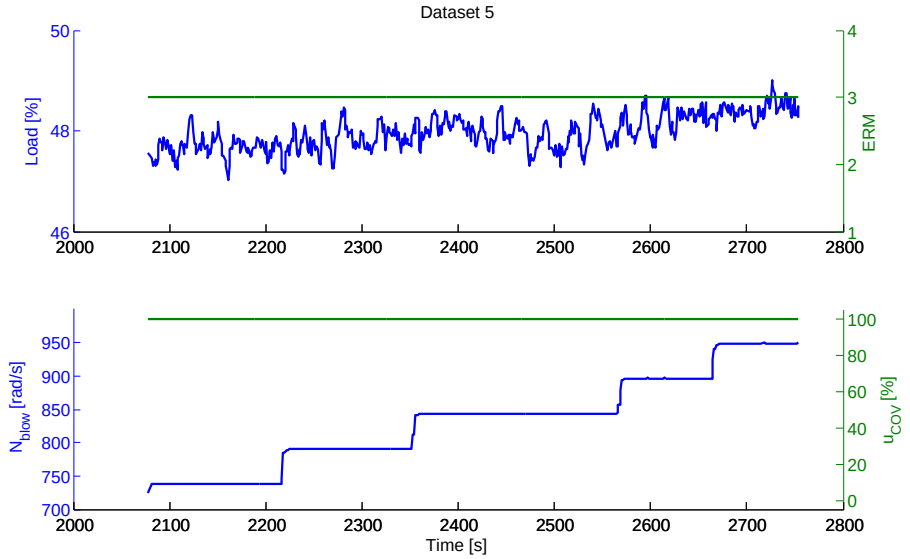

Figure B.2: Input signals from dataset 5

In dataset 6 the engine load is constant at 50% and the EGR system is started up.

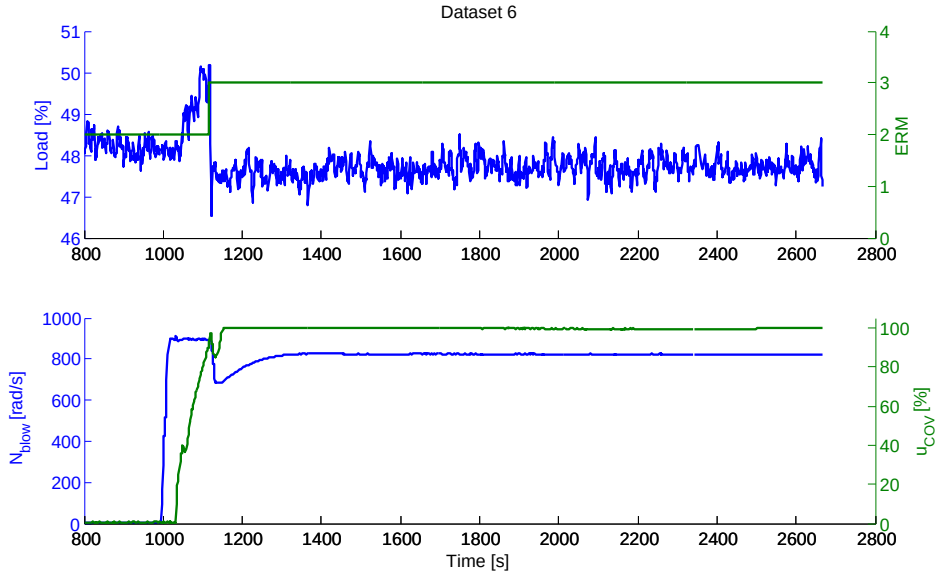

Figure B.3: Input signals from dataset 6

APPENDIX C

Simulation Results

In this appendix the simulation results for datasets: 2, 3, 5 and 6 are shown. Each dataset is shown in a different section

C.1 Simulation results obtained with dataset 2

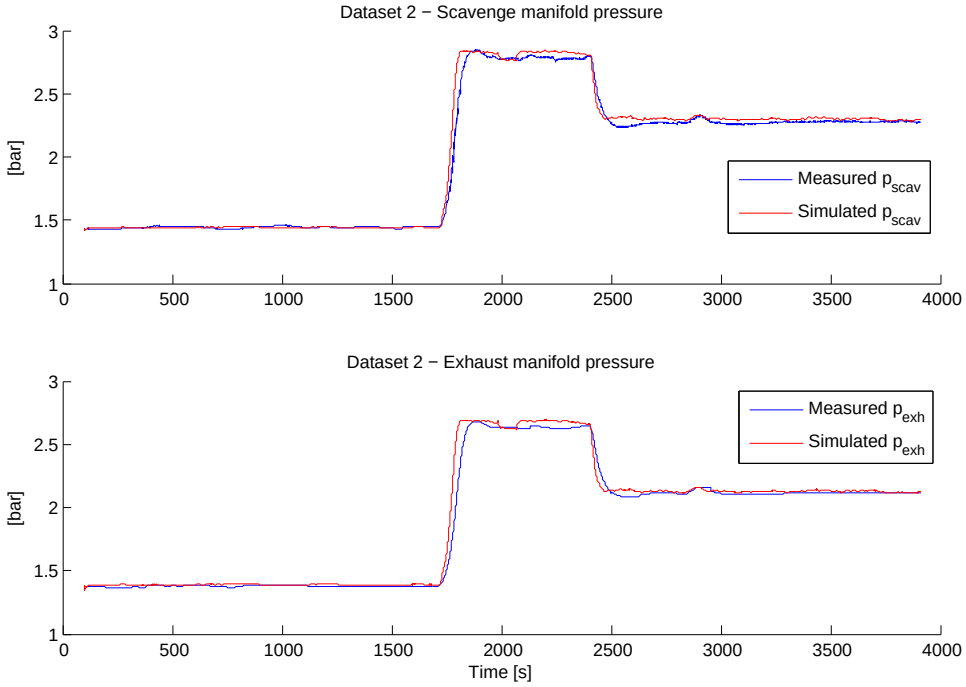

Figure C.1: Comparison between estimated and measured pressures in both manifolds

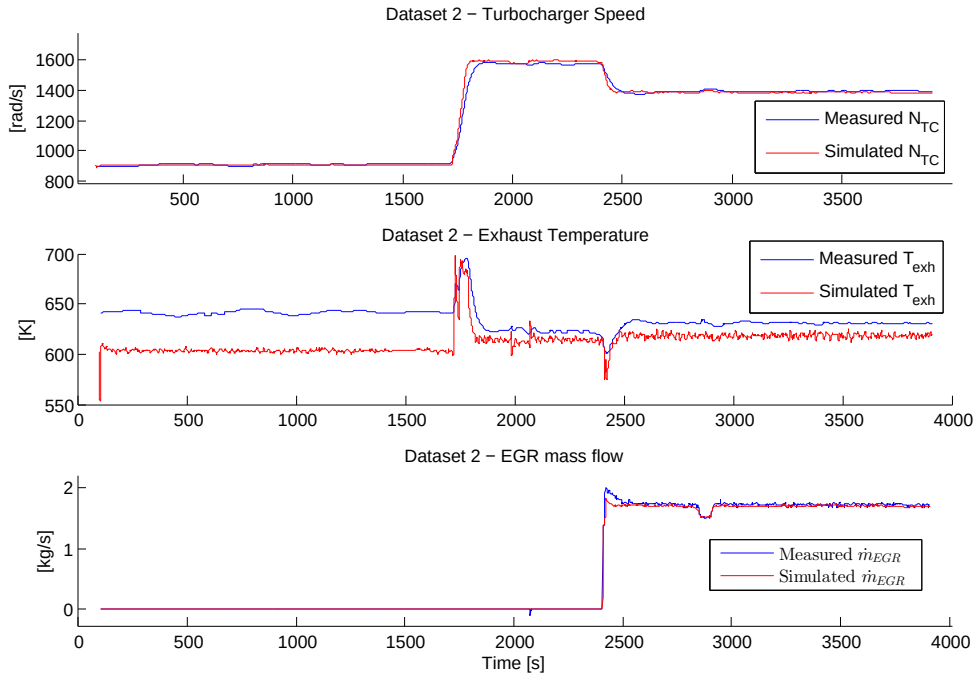

Figure C.2: Comparison between estimated and measured turbocharger speed, exhaust temperature and EGR mass flow

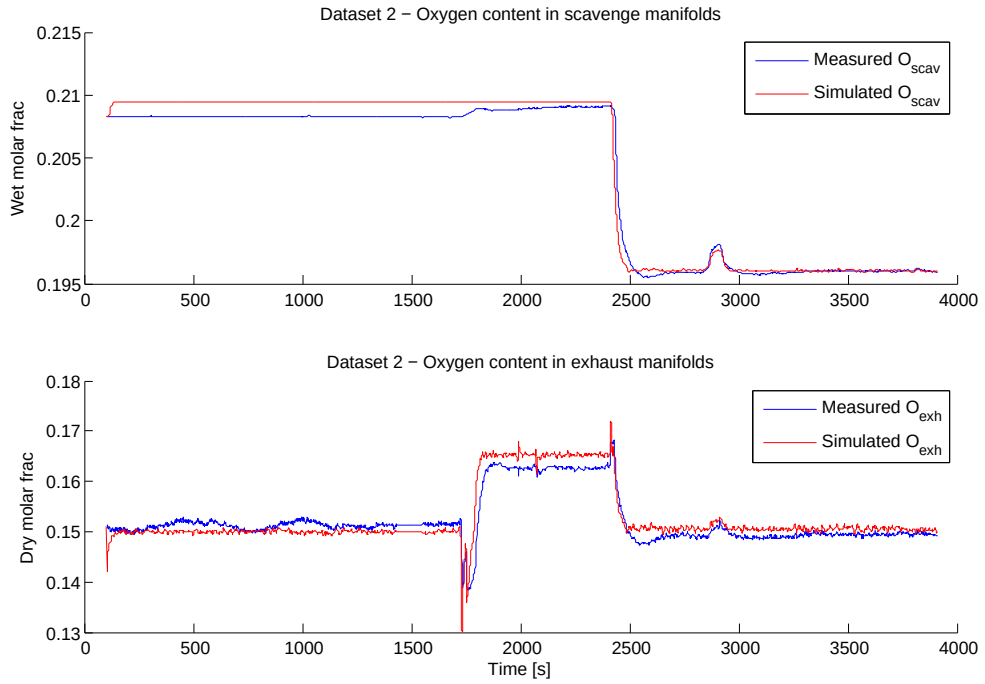

Figure C.3: Comparison between estimated and measured oxygen content in both manifolds

C.2 Simulation results obtained with dataset 3

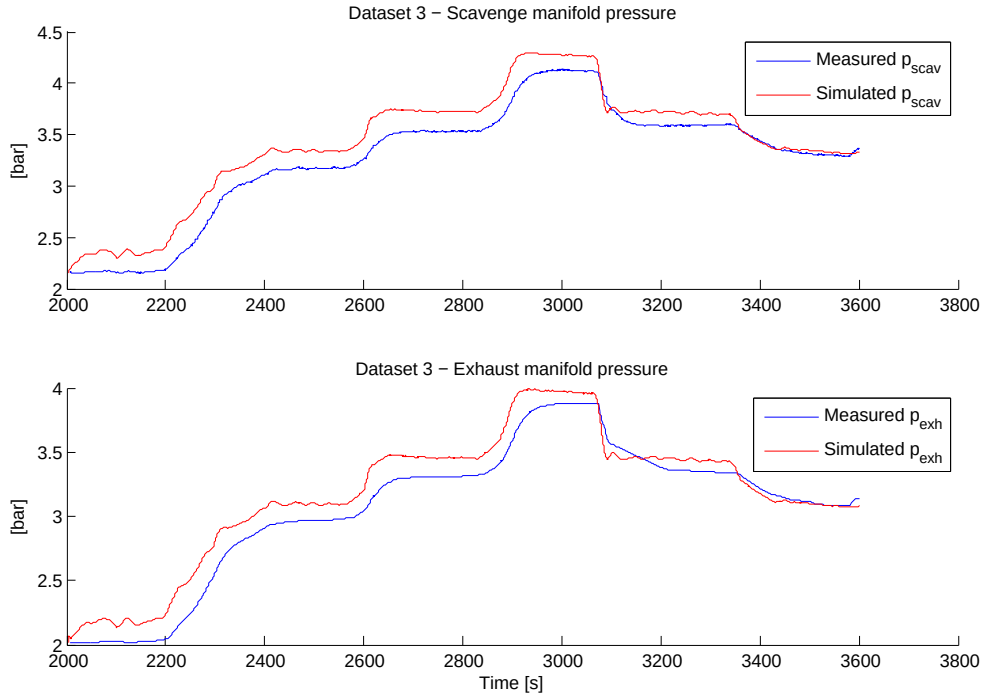

Figure C.4: Comparison between estimated and measured pressures in both manifolds

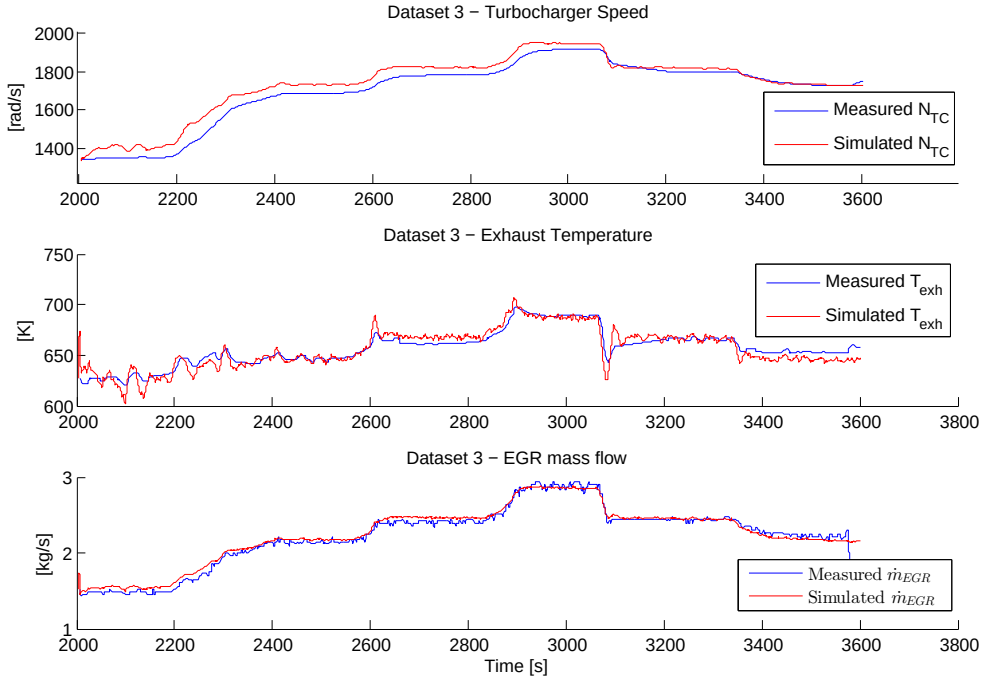

Figure C.5: Comparison between estimated and measured turbocharger speed, exhaust temperature and EGR mass flow

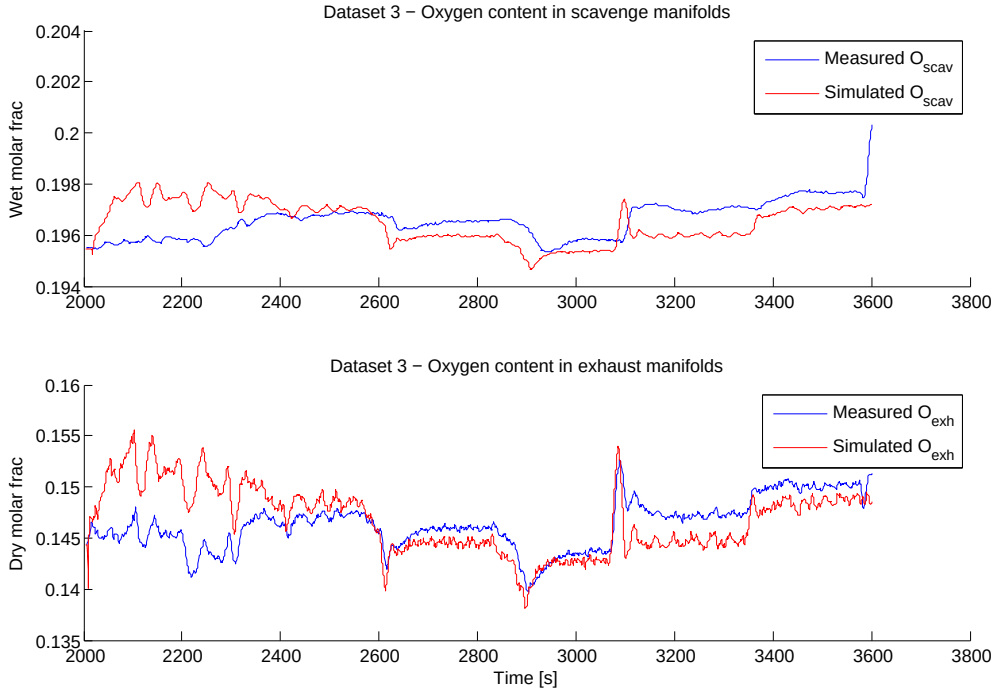

Figure C.6: Comparison between estimated and measured oxygen content in both manifolds

C.3 Simulation results obtained with dataset 5

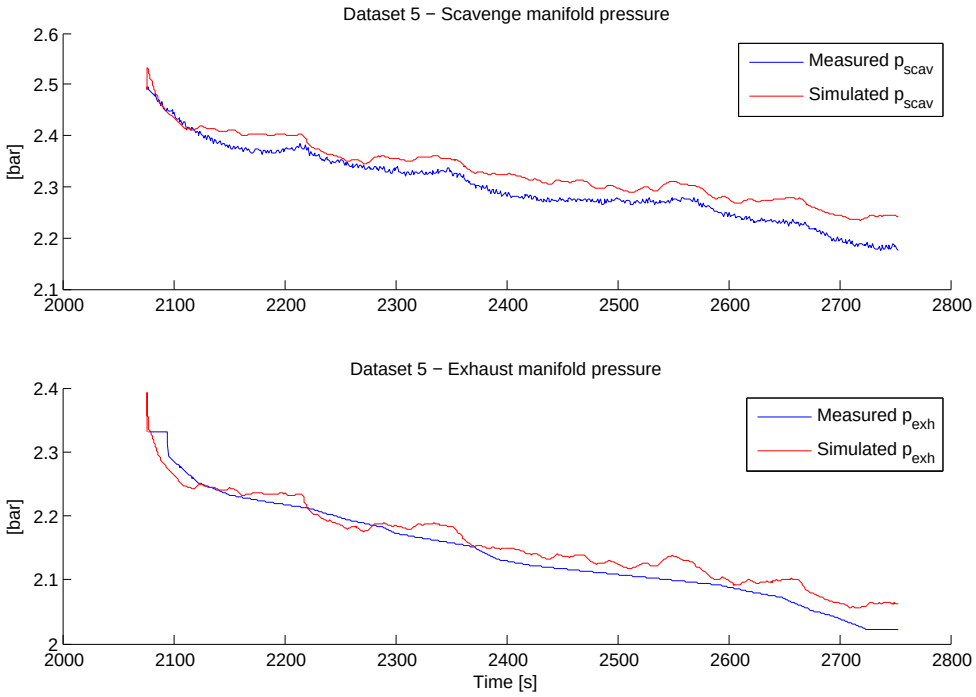

Figure C.7: Comparison between estimated and measured pressures in both manifolds

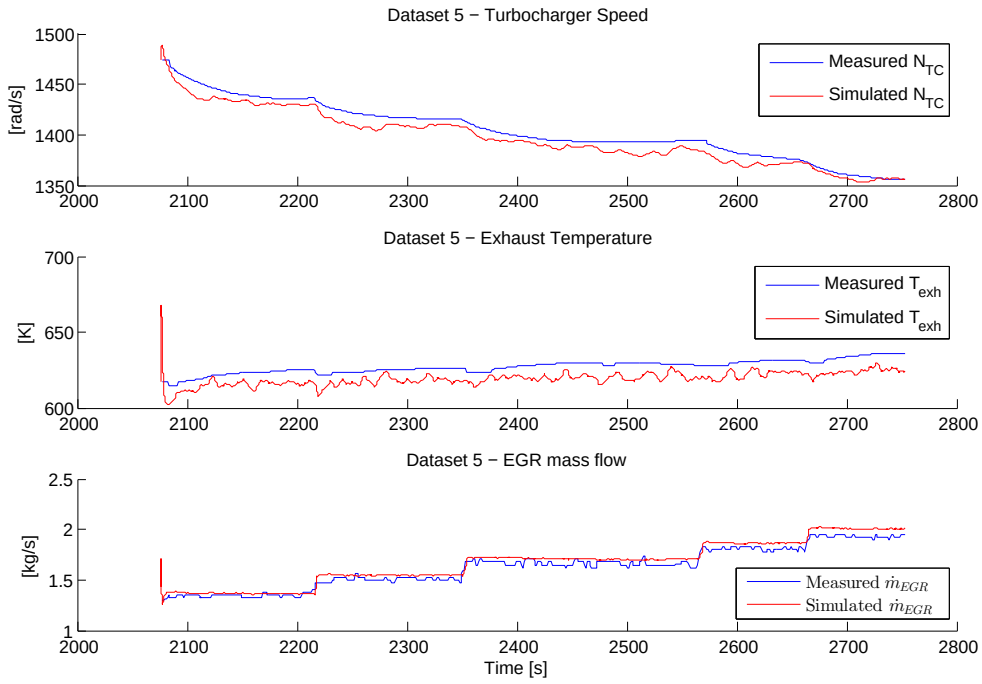

Figure C.8: Comparison between estimated and measured turbocharger speed, exhaust temperature and EGR mass flow

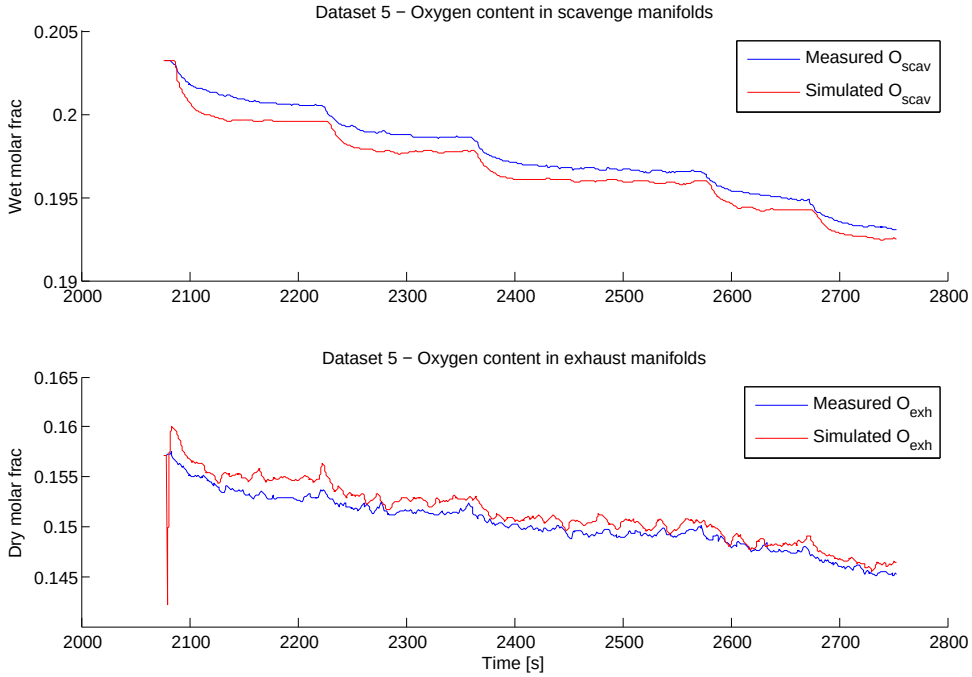

Figure C.9: Comparison between estimated and measured oxygen content in both manifolds

C.4 Simulation results obtained with dataset 6

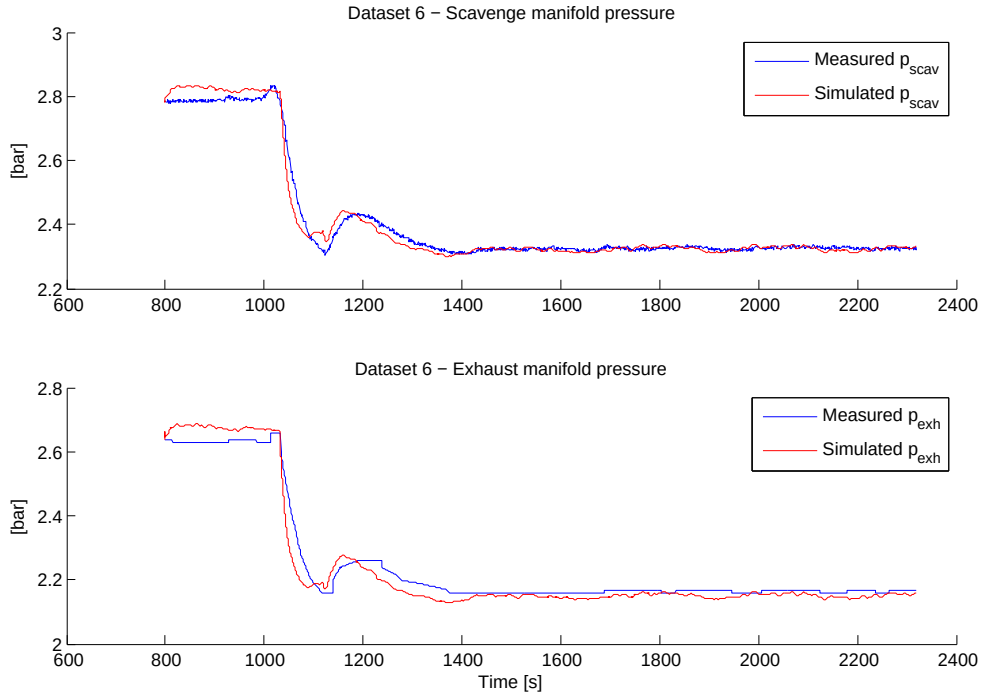

Figure C.10: Comparison between estimated and measured pressures in both manifolds

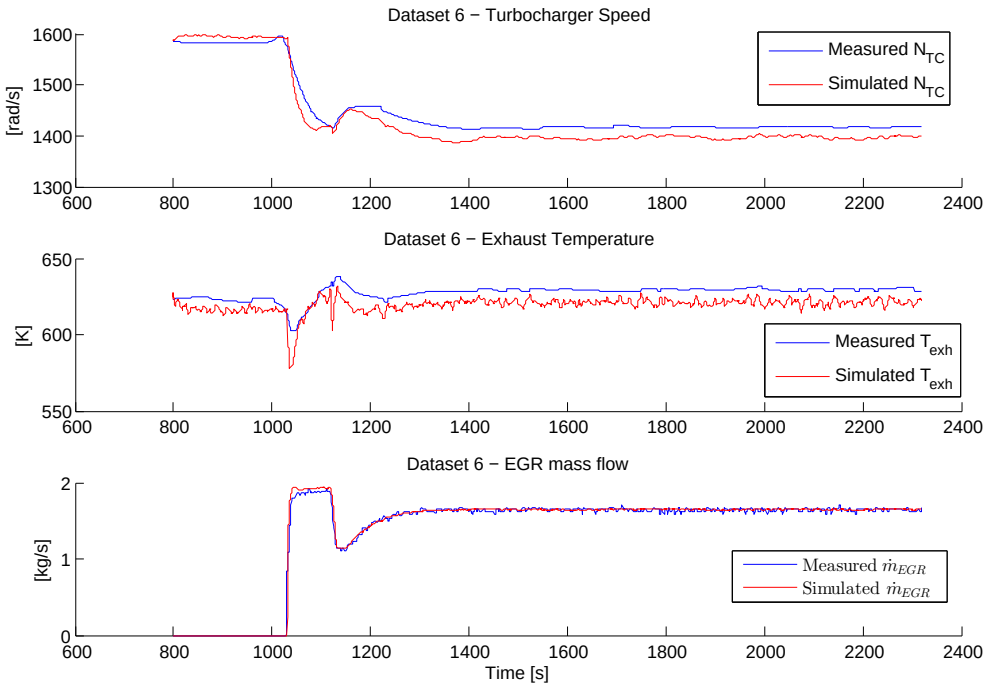

Figure C.11: Comparison between estimated and measured turbocharger speed, exhaust temperature and EGR mass flow

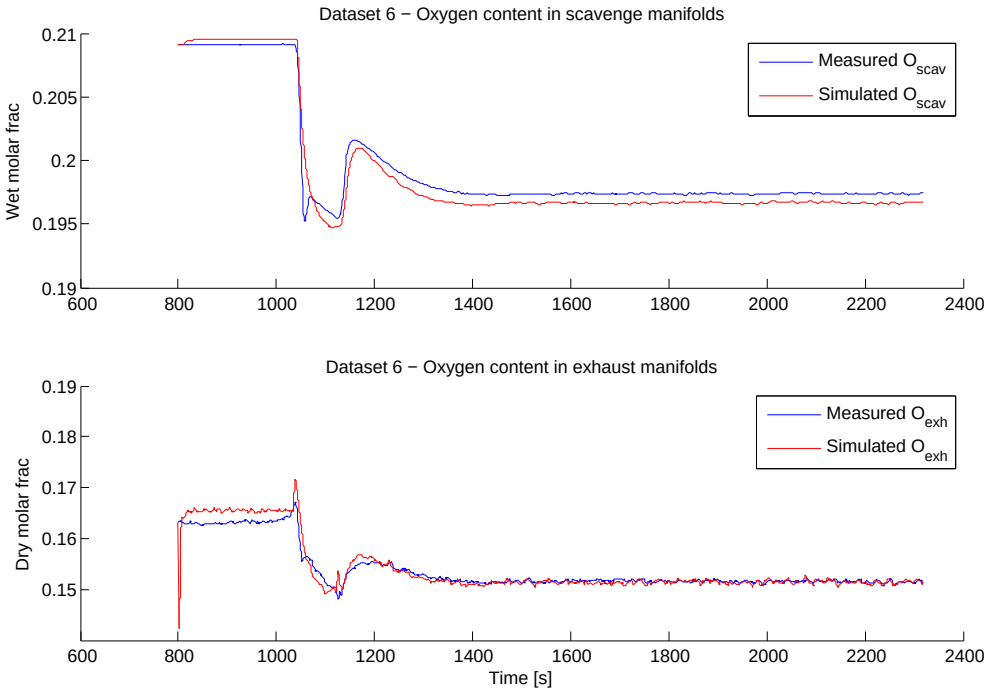

Figure C.12: Comparison between estimated and measured oxygen content in both manifolds

DTU Mechanical Engineering
Section of Thermal Energy
Technical University of Denmark

Nils Koppels Allé, Bld. 403
DK- 2800 Kgs. Lyngby
Denmark
Phone (+45) 4525 4131
Fax (+45) 4588 4325

www.mek.dtu.dk